

1 **Enhanced simulated early 21st century Arctic sea ice loss due to CMIP6 biomass**
2 **burning emissions**

3 Short Title: Biomass burning impact on Arctic sea ice loss

4 **Authors**

5 Patricia DeRepentigny^{1,2*†}, Alexandra Jahn^{1,2}, Marika M. Holland³, Jennifer E. Kay^{1,4}, John
6 Fasullo³, Jean-François Lamarque³, Simone Tilmes⁵, Cécile Hannay³, Michael J. Mills⁵, David
7 A. Bailey³, and Andrew Barrett⁶

8 **Affiliations**

9 ¹Department of Atmospheric and Oceanic Sciences, University of Colorado Boulder, Boulder, CO,
10 USA.

11 ²Institute of Arctic and Alpine Research, University of Colorado Boulder, Boulder, CO, USA.

12 ³Climate and Global Dynamics Laboratory, National Center for Atmospheric Research, Boulder,
13 CO, USA.

14 ⁴Cooperative Institute for Research in Environmental Sciences, University of Colorado Boulder,
15 Boulder, CO, USA.

16 ⁵Atmospheric Chemistry Observations and Modeling Laboratory, National Center for Atmospheric
17 Research, Boulder CO, USA.

18 ⁶National Snow and Ice Data Center, University of Colorado Boulder, Boulder, CO, USA.

19

20 *Corresponding author: Patricia DeRepentigny, patricia.derepentigny@colorado.edu

21

22 †Now at the Climate and Global Dynamics Laboratory, National Center for Atmospheric Research,
23 Boulder, CO, USA.

24 **Abstract**

25 The mechanisms underlying decadal variability in Arctic sea ice remain an active area of research.
26 Here we show that variability in boreal biomass burning (BB) emissions strongly influence simu-
27 lated Arctic sea ice on multi-decadal timescales. In particular, we find that a strong acceleration in
28 Arctic sea ice decline in the early 21st century in the Community Earth System Model version 2
29 (CESM2) is related to increased variability in prescribed CMIP6 BB emissions through summer-
30 time aerosol-cloud interactions. Furthermore, we find that the previously reported improvement in
31 sea ice sensitivity to CO₂ emissions and global warming from CMIP5 to CMIP6 can be attributed
32 in part to the imposed increased BB emission variability, at least in the CESM model. These re-
33 sults highlight the complexities of incorporating new observational data into model forcing, while
34 also raising the question of a BB-forced contribution to the observed accelerated early 21st century
35 Arctic sea ice loss.

36 **Teaser**

37 Increased inter-annual variability in CMIP6 prescribed biomass burning emissions in the early 21st
38 century leads to enhanced simulated Arctic sea ice loss.

39 **MAIN TEXT**

40 **Introduction**

41 Arctic sea ice has experienced drastic reductions in extent, thickness and volume in recent decades,
42 making it one of the most striking manifestations of anthropogenic climate change. Sea ice loss
43 has been observed in all months of the year (1) but particularly notable is the loss of late-summer
44 sea ice, with reductions in September ice extent and thickness since 1979 of roughly 45% and
45 66%, respectively (1, 2). The September sea ice extent loss was largest in the early 21st century,
46 reaching -13.3% per decade over the 14-year period of 1993–2006 (3). In contrast, the last 14

47 years have seen a slowdown of the rate of sea ice decline (4), with the 2007–2020 sea ice loss trend
48 decreasing to -4.0% per decade (3).

49 The fact that internal climate variability can produce periods of up to two decades featuring
50 enhanced or negligible sea ice loss even as global temperatures rise is well documented in the
51 scientific literature (5, 6, 7, 8). It is thus possible that the current period of reduced September
52 sea ice trends is due solely to internal variability masking the anthropogenically-induced decline
53 (8). For example, recent work suggests that the inter-decadal variability of Arctic atmospheric
54 circulation related to teleconnections from the eastern-central tropical Pacific contributed to the
55 abrupt warming and Arctic sea ice loss from 2007 to 2012 and the much slower decline in recent
56 years (4). However, it is also possible that there is a previously unidentified forced contribution to
57 the observed change in sea ice loss trends. For instance, a recent model-based analysis revealed
58 that Arctic warming and sea ice loss in the second half of the 20th century have been enhanced
59 by emissions of ozone depleting substances (9). Other studies suggest that reductions in anthro-
60 pogenic aerosols emissions between the 1980s and 2010 may have warmed the Arctic surface
61 (10, 11, 12). Furthermore, the potential of biomass burning emissions from forest fires, which
62 consist of mostly primary organic aerosols, black carbon, and reactive gases, to change the Arctic
63 aerosol population and affect the rate of Arctic sea ice loss has also been brought forward (13, 14),
64 particularly in light of the severe wildfire seasons in recent years (15, 16, 17). In turn, a recent
65 study shows that increasing large wildfires during autumn over the western United States are fu-
66 eled by more fire-favorable weather associated with declines in Arctic sea ice during preceding
67 months (18), emphasizing the complex interactions between fires and Arctic climate change.

68 Emissions from biomass burning (BB) prescribed for the sixth phase of the Climate Model In-
69 tercomparison Project (CMIP6) historical simulations (19) contain a period of strongly enhanced
70 inter-annual variability between 1997–2014. Rather than reflecting an actual sudden increase in
71 BB emission variability, the enhanced variability is due to a change in available observed BB emis-
72 sion data. In CMIP6, satellite-based emissions from the Global Fire Emissions Database (GFED)
73 version 4 with small fires (20) from 1997 to 2014 were combined with either proxy records (when

74 available) or fire models to estimate historical BB emissions starting in 1750 (19). This large in-
75 crease in variability starting in 1997 is new to the CMIP6 forcing and was not present in CMIP5
76 where decadal means were used to construct historical gridded BB emissions (21), such that the
77 change in variability in the source datasets at the start of the GFED era did not affect the variability
78 of prescribed emissions. Here we show that the increased inter-annual variability in prescribed
79 CMIP6 historical BB emissions from wildfires starting in 1997 leads to an acceleration of simu-
80 lated early 21st century Arctic sea ice loss in the CESM2 Large Ensemble (CESM2-LE) (22) due to
81 non-linear aerosol-cloud interactions during the melt season. We identify this link by performing
82 sensitivity experiments in which we remove the increased BB variability from the CMIP6 historical
83 forcing while conserving the total integrated amount of BB emissions from 1997–2014. In order to
84 isolate forced contributions to the Arctic sea ice evolution, we primarily focus on ensemble means,
85 which reflect the model response to external forcing. We further show how this affects simulated
86 sea ice sensitivities in the CESM, before discussing the implications of these model-based findings
87 for the CMIP6 effort and the potential relevance for the observed evolution of Arctic sea ice.

88 **Results**

89 **Accelerated sea ice loss in the CESM2-LE compared to the CESM1-LE**

90 The evolution of Arctic sea ice area in September throughout the 20th and 21st centuries differs
91 greatly between the CMIP5-forced version of the CESM, the CESM1-LE (23), and the CMIP6-
92 forced version, the CESM2-LE (22) (Fig. 1A). Even before the start of the decline in Arctic sea ice
93 in the later part of the 20th century, the two CESM versions have a large mean state difference, with
94 the CESM1-LE simulating a thicker and more extensive sea ice cover compared to the CESM2-LE
95 (24). In addition to this mean state difference, there is a statistically significant difference in the
96 rate of Arctic sea ice loss starting in the mid-1990s (Fig. 1, B and C). The CESM1-LE September
97 sea ice area anomaly and trend are gradually more negative with time until the Arctic reaches
98 ice-free conditions every year (25). In contrast, the sea ice cover in the CESM2-LE experiences

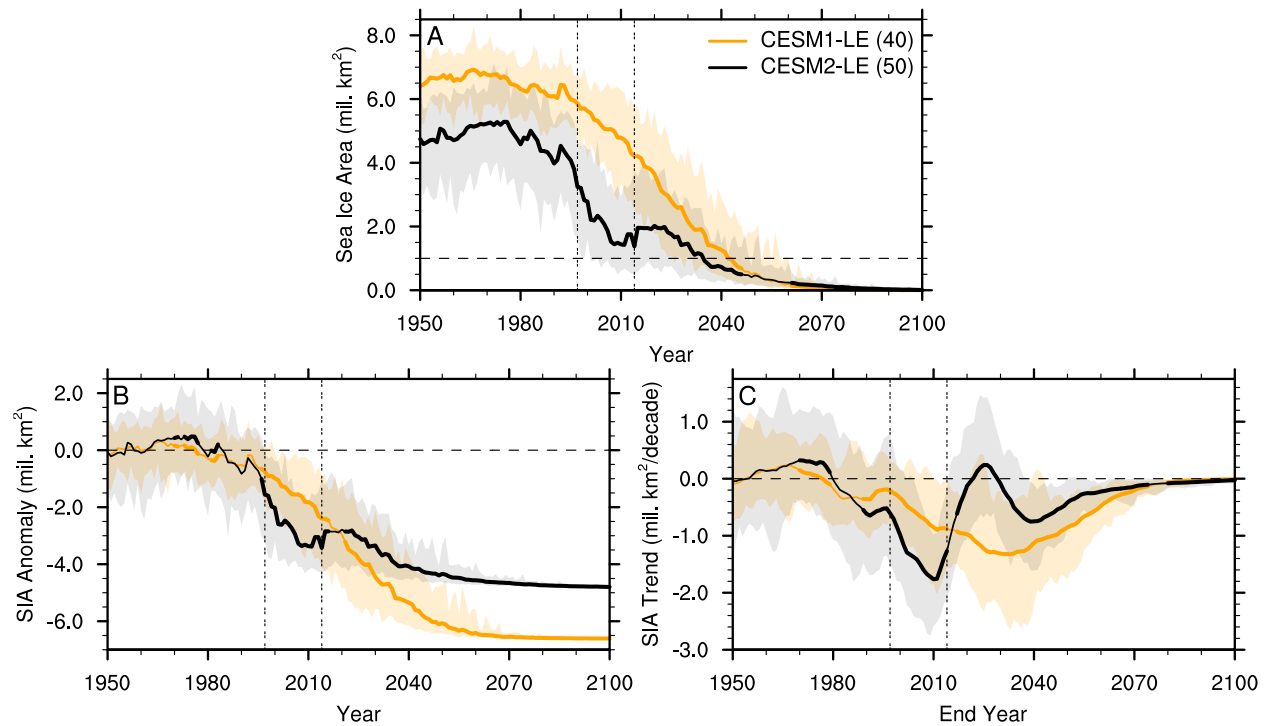


Fig. 1. Differences in the rate of Arctic sea ice loss. September (A) sea ice area (SIA), (B) SIA anomalies relative to the 1940–1969 average, and (C) 20-year linear SIA trends in the CESM1-LE and the CESM2-LE (the ensemble size is indicated in parentheses in the legend). The ensemble mean is shown by the solid line, the full ensemble range is shown by the shading, the horizontal dashed line indicates ice-free conditions in (A), no anomalies in (B) and no trend in (C), and the two vertical double-dashed lines indicate the GFED period. Years when the CESM1-LE and the CESM2-LE are statistically different at the 95% significance level are indicated with a thicker ensemble mean line and are determined using a two-sample Welch’s t-test. In (C), values on the x-axis indicate the end year of the 20-year period over which the linear trend is computed.

99 a sharp decline in area starting in the mid-1990s up until the end of the first decade of the 21st
 100 century (Fig. 1B), with the ensemble mean sea ice loss trend reaching its highest value of about
 101 -1.8 million $\text{km}^2/\text{decade}$ around end year 2010 (Fig. 1C). This is followed by a decade-long
 102 sea ice recovery in the CESM2-LE ensemble mean until ~ 2025 characterized by neutral or even
 103 positive trends, after which the ensemble mean area anomaly and trend continue to become more
 104 negative until the sea ice cover melts out completely every summer (24). Note that this feature of
 105 the CESM2-LE sea ice evolution is present regardless of the choice of future CMIP6 emissions
 106 scenario (24), in all months of the year (Fig. S1; although it is most pronounced at the end of
 107 the summer), as well as in the version of the CESM2 that uses a high-top atmosphere model,

108 WACCM6, instead of the standard CESM2 atmosphere model, CAM6 (24).

109 **Impact of BB emissions on simulated Arctic climate**

110 We find that the change in prescribed BB emissions from CMIP5 to CMIP6 can explain much of
111 the difference in Arctic sea ice evolution between the CESM1-LE and the CESM2-LE. Previous
112 studies suggest that the aerosol forcing of CMIP5 simulations might have been too weak in recent
113 decades (26, 27). In CMIP6, BB emissions were updated to include inter-annual variability (19),
114 rather than using decadal means (21) (Fig. 2). Although this decision allows for a more realistic
115 depiction of BB emissions over the historical period, it also results in a sudden increase of the inter-
116 annual variability in BB emissions in 1997 at the start of the GFED era (Fig. 2). This increase in
117 variability is especially pronounced in the Northern Hemisphere (NH) mid-latitudes, where the
118 variability increases by a factor of five compared to pre-GFED years (defined here as 1950–1996;
119 Fig. 2A). The inter-annual variability in global BB emissions increases as well, although only by a
120 factor of two (Fig. 2B).

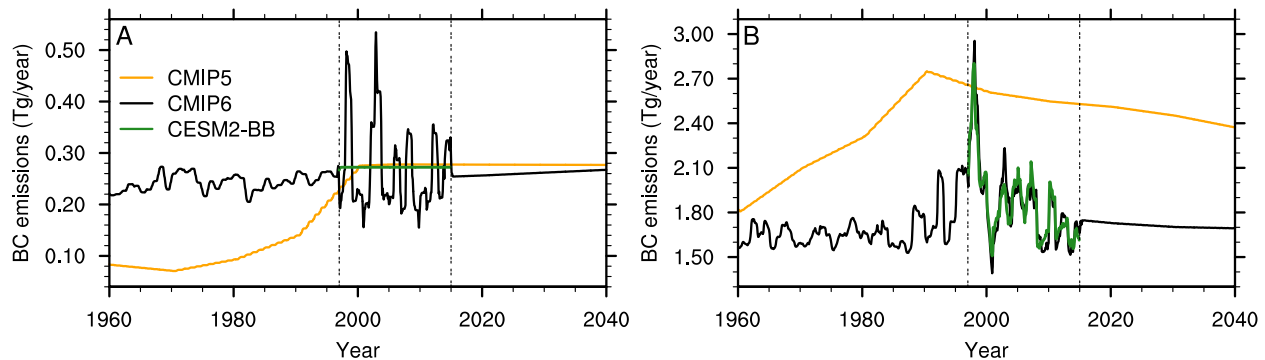


Fig. 2. Changes in BB forcing. Prescribed total black carbon emissions from BB (A) between 40–70°N and (B) globally in CMIP5, CMIP6 and the CESM2-BB, smoothed with a 12-month running mean. The two vertical double-dashed lines indicate the GFED period. Note that the range of values on the y-axis is different between the two panels, with higher values of total global black carbon emissions. Here we used black carbon emissions to represent BB emissions as it is the most radiatively important one, but all other prescribed BB emissions (dimethyl sulfide, primary organic matter, sulfur dioxide, sulfate aerosols and secondary organic aerosols) follow a similar time evolution as black carbon (not shown).

121 To isolate the impact of the increased BB variability over the GFED era on Arctic sea ice,
122 we conducted sensitivity ensemble simulations (referred to as CESM2-BB hereafter) in which

123 the inter-annual variability in BB emissions from 1997–2014 between 40–70°N is removed but
124 the integrated amount of emissions over that same period is retained (Fig. 2A; see Materials and
125 Methods for details). As a result, the CESM2-BB has prescribed BB emissions over the NH
126 mid-latitudes that are more similar to CMIP5 during the GFED period, with emissions pre- and
127 post-GFED being the same as in CMIP6 (Fig. 2A). Because NH mid-latitude BB emissions make
128 up only ~14% of the global BB emissions, the variability of global BB emissions is practically
129 unchanged in the CESM2-BB compared to CMIP6 (Fig. 2B).

130 The sensitivity experiments show that the warming of the Arctic (70–90°N) over the GFED pe-
131 riod is more pronounced in the CESM2-LE compared to the CESM2-BB (Fig. 3A), with the largest
132 difference over the central and Pacific sectors of the Arctic Ocean (Fig. S3, A and B). Specifically,
133 the 20-year linear trends in Arctic surface air temperature in the CESM2-LE are significantly larger
134 than the CESM2-BB over most of the GFED period (Fig. 3B), after which the trends reduce to neu-
135 tral values in the ensemble mean until around end year 2025. In addition, the September Arctic sea
136 ice area anomaly and trends are reduced (i.e., less negative) in the CESM2-BB compared to the
137 CESM2-LE over the GFED period (Fig. 3, C and D). Similar results are found not just at the sea
138 ice minimum but in all months of the year, although the difference between the CESM2-BB and
139 the CESM2-LE is most pronounced from July to November (Fig. S1). This reduction in the rate
140 of Arctic sea ice decline over the GFED era in the CESM2-BB is not limited to a specific region,
141 but is present everywhere in the central Arctic Ocean and particularly over the Pacific sector of
142 the Arctic (Fig. S3, C and D). As only the inter-annual variability in BB emissions over the GFED
143 period differs between the two ensembles, these results allow us to conclude that the increased
144 BB variability in CMIP6 over the GFED period is causing enhanced Arctic warming and sea ice
145 decline since the late 1990s in the CESM2-LE. Note that the impact of the increased variability of
146 BB emissions is not limited to the Arctic, but is also present north of 30°N, particularly over land,
147 as shown in a companion paper that uses the same sensitivity simulations (28).

148 The impact of BB emissions on Arctic climate can be explained by aerosol-cloud interactions
149 (Fig. 4). Freshly emitted BB particles are specified to be hydrophobic (primary carbon mode) in

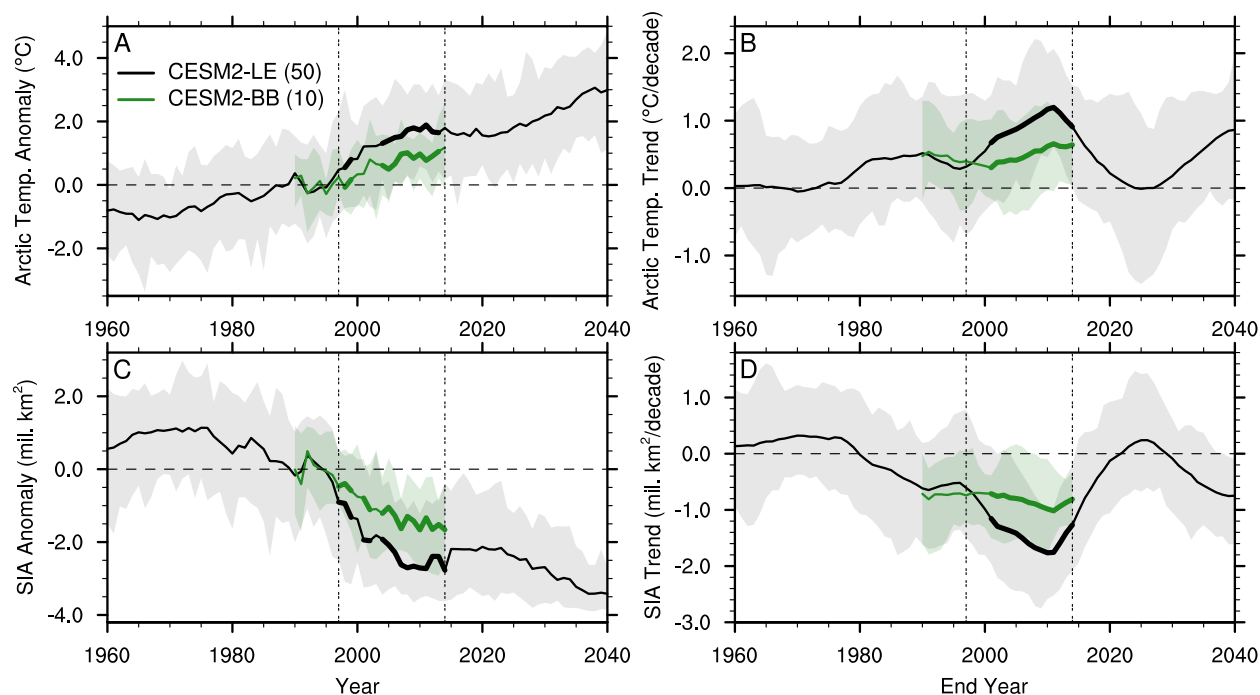


Fig. 3. BB emissions impact on Arctic climate. Annual Arctic ($70\text{--}90^\circ\text{N}$) surface air temperature (A) anomalies relative to the 1990–1996 average (when the two simulations share the same forcing) and (B) 20-year linear trends, and September sea ice area (SIA) (C) anomalies relative to the 1990–1996 average and (D) 20-year linear trends in the CESM2-LE and the CESM2-BB (the ensemble size is indicated in parentheses in the legend). The ensemble mean is shown by the solid line, the full ensemble range is shown by the shading, the horizontal dashed line indicates no anomalies in (A and C) and no trend in (B and D), and the two vertical double-dashed lines indicate the GFED period. Years when the CESM2-LE and the CESM2-BB are statistically different at the 95% significance level are indicated with a thicker ensemble mean line and are determined using a two-sample Welch’s t-test. Note that while the CESM2-BB has a smaller ensemble size than the CESM2-LE (10 versus 50 ensemble members), its ensemble size is sufficient to detect a forced sea ice response to the modified BB emissions (Fig. S2, C and D). In (B and D), values on the x-axis indicate the end year of the 20-year period over which the linear trend is computed.

150 the CESM model and as such cannot initially serve as cloud condensation nuclei (CCN). Through
 151 microphysical aging processes, these BB particles gradually become hydrophilic (29, 30). We
 152 find that the inter-annual variability in BB emissions over the NH mid-latitudes in the CESM2-LE
 153 (Fig. 2A) is reflected in the Arctic summertime number concentration of aerosols in the primary
 154 carbon mode (Fig. S4), showing that fresh BB aerosols from those emissions are advected to the
 155 Arctic. However, the signature of the inter-annual variability in BB emissions is partly lost for
 156 the aged aerosols (i.e., those that can act as CCN; Fig. 4A). Specifically, years with smaller BB

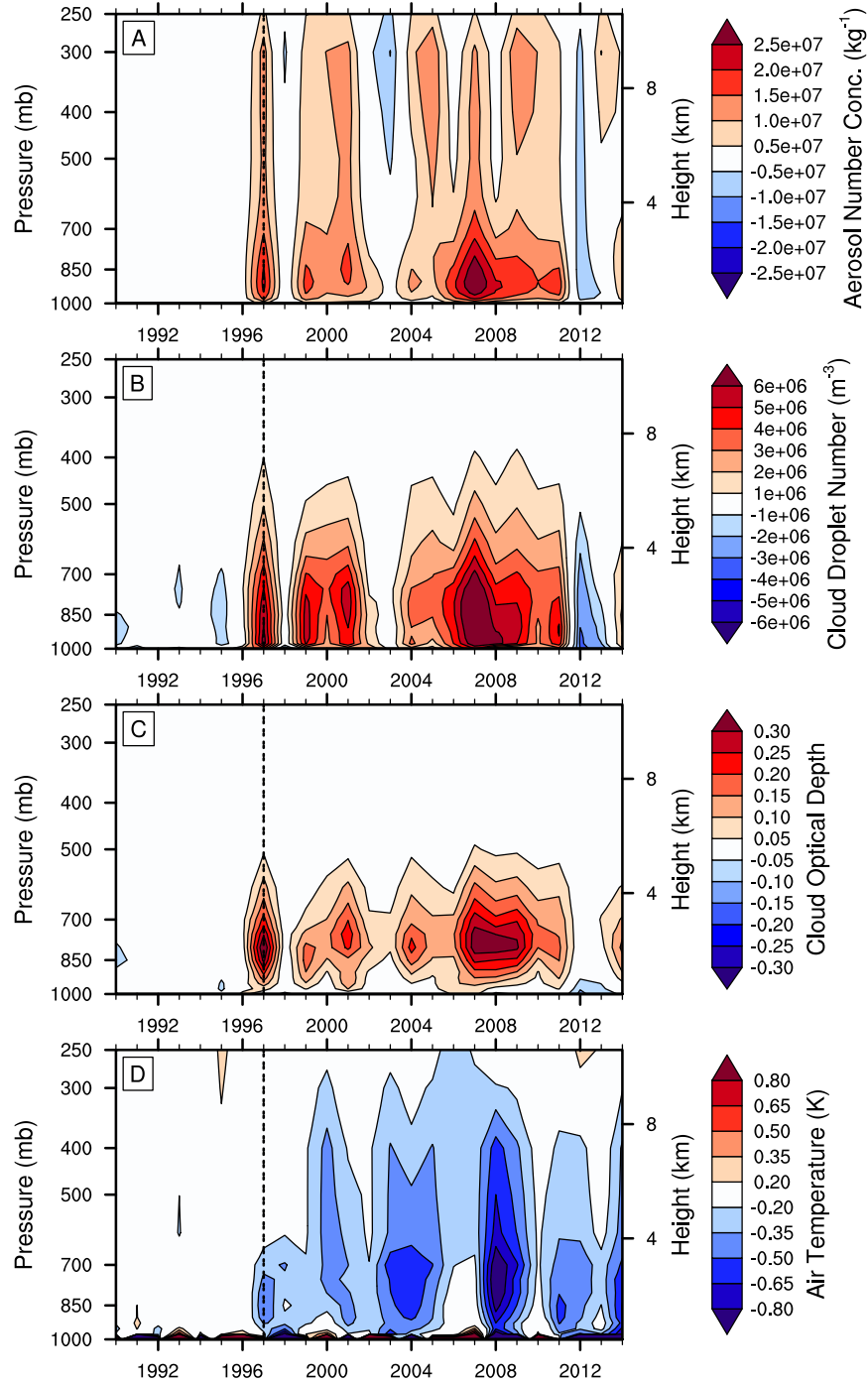


Fig. 4. BB emissions impact on Arctic aerosol-cloud interactions. Difference (CESM2-BB – CESM2-LE) in Arctic (70–90°N) summer (JJA) (A) number concentration of aerosols in the accumulation mode, (B) cloud condensation nuclei (CCN) concentration, (C) cloud optical depth and (D) air temperature with height. Positive differences (red) indicate larger values in the CESM2-BB and negative differences (blue) indicate larger values in the CESM2-LE. The vertical double-dashed line indicates the start of the GFED period.

157 emissions in the CESM2-LE compared to the CESM2-BB (i.e., 1997, 1999–2001, 2004–2011; see
158 Fig. 2A) result in lower Arctic summertime number concentration of aerosols in the accumulation
159 mode. Indeed, the larger aerosol emissions in the CESM2-BB during those years lead to larger
160 aerosol numbers with smaller aerosol diameter (not shown) compared to the CESM2-LE (Fig. 4A).
161 But the opposite is not true for years with larger BB emissions in the CESM2-LE than in the
162 CESM2-BB (i.e., 1998, 2002–2003, 2012–2014; see Fig. 2A). During those years, there is very
163 little difference between the two CESM simulations in terms of aerosol number concentration
164 (Fig. 4A). This asymmetric response is likely a reflection of the observed non-linear and saturated
165 response of CCN to aerosol loading (31, 32). Indeed, it has been previously shown that cloud
166 albedo has a non-linear response to aerosol emissions that diminishes with increasing emissions
167 (32, see their Fig. 3). As a result of the larger concentration of summertime aerosols in the
168 accumulation mode in the CESM2-BB in years with larger NH mid-latitude BB emissions, we
169 find larger cloud droplet number concentration in the CESM2-BB compared to the CESM2-LE,
170 especially close to the surface and up to about 500 mb (Fig. 4B). This results in higher lower-
171 tropospheric cloud optical depth compared to the CESM2-LE over the GFED period (Fig. 4C)
172 through indirect aerosol-cloud interactions, specifically the Twomey effect (33). The higher cloud
173 optical depth is associated primarily with increases in cloud liquid amount (Fig. S5) and leads to
174 a net cooling from the surface up to about 300 mb (Fig. 4D). Although the local impact of an
175 increased aerosol loading in the Arctic is the non-linear result of competing cooling and warming
176 aerosol indirect effects (14), the decrease in Arctic surface reflectivity during the melting season
177 shifts the aerosol indirect effect towards cooling (34). Note that the temperature response towards
178 the end of the GFED period is likely enhanced through snow/ice albedo feedback as the extent of
179 the sea ice cover start to significantly differ between the two ensembles (Fig. 3C).

180 **Impact of BB emissions on sea ice sensitivity**

181 The observed loss of Arctic sea ice has been shown to be tightly coupled to increasing global mean
182 surface air temperature (35, 36, 37) and cumulative anthropogenic CO₂ emissions (38). This metric

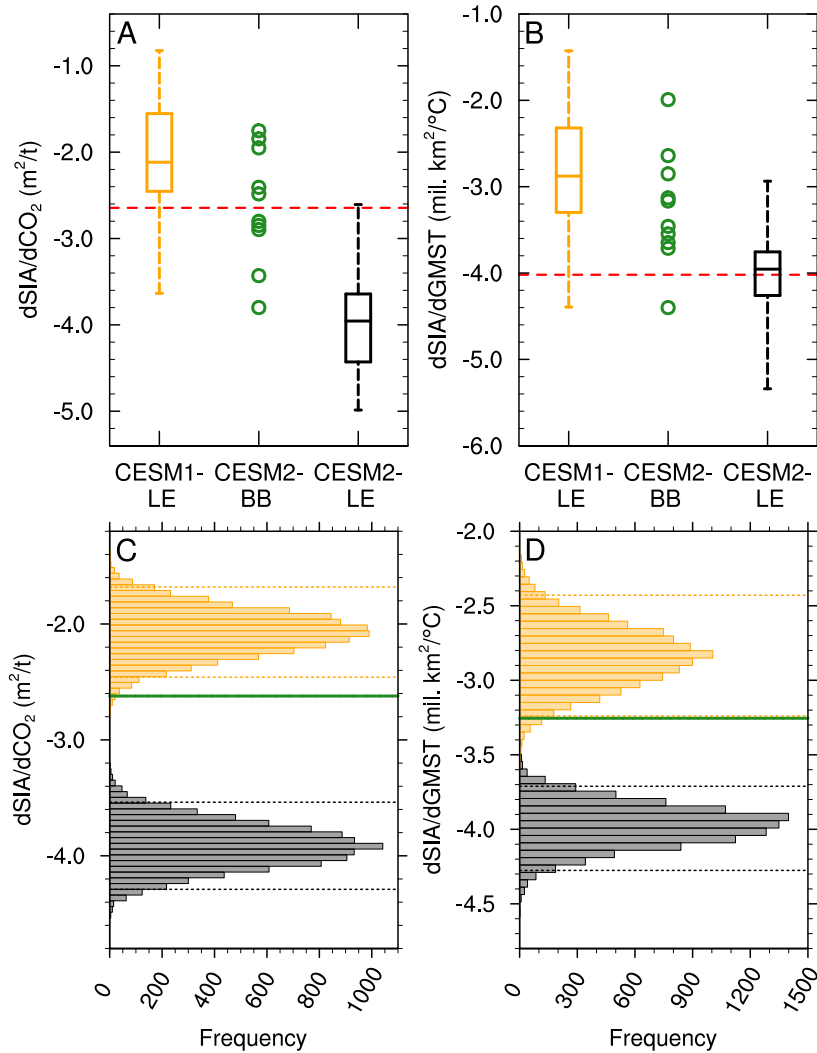


Fig. 5. BB emissions impact on sea ice sensitivity. Sea ice sensitivity to (A) cumulative anthropogenic CO₂ emissions (defined as the change in Arctic September sea ice area per change in cumulative anthropogenic CO₂ emissions in m² per tonne of CO₂) and (B) global annual mean surface temperature (defined as the change in Arctic September sea ice area per change in global mean surface temperature in million km² per °C) from 1979–2014 in the CESM1-LE, the CESM2-BB and the CESM2-LE, with the red dashed line showing the observed sensitivity. For the two large ensembles, the box shows the inter-quartile range, the line inside the box shows the median, and the whiskers show the minimum and maximum across all ensemble members, and for the CESM2-BB the green circles indicate the sea ice sensitivity of the 10 ensemble members. Histograms of sea ice sensitivity to (C) cumulative anthropogenic CO₂ emissions and (D) global annual mean surface air temperature obtained by bootstrapping the CESM1-LE and CESM2-LE ensemble means with 10 members 10,000 times, with the dotted lines showing the 95% confidence range for each distribution and the green line indicating the ensemble mean sensitivity of the CESM2-BB.

183 of sea ice sensitivity to CO₂ and global warming is commonly used by the sea ice community
 184 and has even been proposed as a way to reduce the uncertainty range of future sea ice evolution

185 (38, 39). Previous literature has shown that models usually simulate a lower sensitivity of Arctic
186 sea ice loss per degree of global warming than has been observed (36, 38, 40) and simulated Arctic
187 sea ice retreat has been found to be accurate only in runs that have too much global warming,
188 which suggests that models may be getting the right Arctic sea ice retreat for the wrong reasons
189 (40). More recently, the CMIP6 multi-model ensemble mean was shown to provide a more realistic
190 estimate of the sensitivity of September Arctic sea ice area to a given amount of anthropogenic CO₂
191 emissions and global warming compared with earlier CMIP experiments (41). It was, however,
192 unclear whether this change reflects an improvement of model physics or primarily arises from
193 differences in the historical forcing in CMIP6 relative to CMIP5, in particular differences in BB
194 emissions and ozone (41).

195 In agreement with what was reported for CMIP6 models as a group (41), we find that the sea
196 ice sensitivity to cumulative anthropogenic CO₂ emissions and global mean surface temperature
197 is generally higher in the CMIP6-forced version of the CESM, the CESM2-LE, compared to the
198 CMIP5-forced version, the CESM1-LE (Fig. 5, A and B). In contrast, the sea ice sensitivities of
199 the CESM2-BB falls somewhere in between the range of sea ice sensitivities of the CESM1-LE
200 and the CESM2-LE, although all 10 ensemble members of the CESM2-BB overlap with at least
201 one of the large ensemble distributions if not both. Note that trends in September sea ice area and
202 global mean surface temperature are related in these simulations, with more sea ice loss present in
203 simulations with more global warming. As such, the change in sea ice sensitivity to global mean
204 surface temperature in the CESM2-BB is influenced by both factors. Using bootstrapping, we show
205 that the sea ice sensitivity of the CESM2-BB ensemble is statistically distinct from the CESM1-LE
206 and the CESM2-LE at the 95% confidence level when accounting for the different ensemble size
207 of the three CESM simulations (Fig. 5, C and D). Note that bootstrapping, or randomly resampling
208 with replacement to generate statistics, requires no distribution assumptions and is only possible
209 with sufficiently large ensembles. Hence, based on results from the CESM model, the increased
210 variability in BB emissions from CMIP5 to CMIP6 seems to be responsible in part for the increased
211 sea ice sensitivity to CO₂ and global warming recently reported by the SIMIP Community (41),

212 with the rest related to other changes in historical forcing and/or improvement of model physics.
213 This is especially true for the sea ice sensitivity to CO₂, as temperature is also affected by the
214 change in BB emissions but CO₂ concentrations are typically prescribed in CMIP6 simulations.

215 **Discussion**

216 We showed that a large part of the enhanced early 21st century Arctic surface warming and Septem-
217 ber sea ice decline in the CESM2-LE compared to the CESM1-LE can be attributed to the increased
218 inter-annual variability in prescribed NH mid-latitude BB emissions during the GFED period in
219 the CMIP6 forcing. Specifically, we showed that the increased BB variability enhances warming
220 due to non-linear aerosol-cloud interactions, as decreased cloud optical depth during years with
221 low BB-related aerosol burdens enhances warming more than years with high BB-related aerosol
222 burdens lead to cooling. Hence, the increased BB variability over the GFED period leads to an
223 additional forced sea ice loss in the CESM2-LE beyond the one driven by increases in greenhouse
224 gases (42) and internal variability (6, 43, 44).

225 The presence of this non-greenhouse gas forced sea ice loss in the early 21st century in models
226 also affects the sea ice sensitivity, a metric often used to evaluate model performance (25, 37, 38,
227 41). Specifically, we find that the increased inter-annual variability in BB emissions during the
228 GFED era explains part of the increase in sea ice sensitivity to CO₂ emissions and global warming
229 from the CMIP5-forced to the CMIP6-forced versions of the CESM. This is the second time that
230 aerosol-related forcing changes have been shown to impact Arctic sea ice trends between CMIP
231 generations (45), highlighting how sensitive sea ice is to the effects of aerosol emissions.

232 Interestingly, it is not only the CESM2 that shows an increase of the rate of Arctic sea ice de-
233 cline over the GFED period, but some other CMIP6 models do as well (Figs. S6 and S7). From the
234 12 additional CMIP6 models assessed here (see Materials and Methods), four (ACCESS-ESM1.5,
235 FGOALS-g3, MIROC6 and MPI-ESM1.2-HR) show an accelerated ensemble mean sea ice loss
236 over the GFED period, although none of them as large as the CESM2. This indicates that the im-
237 pact of BB emissions is likely not just limited to the CESM2 but may affect other CMIP6 models,

238 in agreement with results from a companion paper that finds increased surface downwelling short-
239 wave radiation during the GFED period in several CMIP6 models in addition to the CESM2 (28).
240 The fact that some CMIP6 models show a similar sea ice loss acceleration as the one attributed to
241 the new BB emissions in the CESM2 while others do not calls for a better understanding of inter-
242 model differences in light of their sensitivity to aerosol emissions. Furthermore, the sensitivity
243 of the CESM2 to changes in BB variability raises the question as to whether the lack of inter-
244 annual variability in aerosol forcing in the pre-industrial control and future scenario runs could be
245 problematic.

246 Overall, our analysis shows that BB emissions can influence multi-decadal variations in Arctic
247 sea ice. This work also demonstrates that changes in the variability of emissions, not just changes
248 in the mean, can have large effects on climate through non-linear cloud feedbacks. As such, our
249 findings suggest that the way short-lived climate forcings like BB emissions are prescribed in mod-
250 els can have unexpected remote effects in vulnerable regions such as the Arctic. This highlights the
251 challenges associated with incorporating newly available observations into climate forcing datasets
252 and the importance of avoiding temporal discontinuities, which may help guide decisions in future
253 phases of CMIP. To avoid a sharp increase in BB variability in 1997 while still making use of the
254 new satellite-based observations over the GFED period, we recommend re-assessing the variability
255 of emissions pre-GFED, potentially through the use of an interactive fire model.

256 Finally, the early GFED period stands out as particularly variable in BB emissions north of
257 40°N, both in the real world and in the CMIP6 forcing (19). As discussed earlier, several studies
258 have documented a steepening of the observed trend of Arctic sea ice decline since the mid-1990s
259 (46, 47) and a smaller trend since 2007 (3, 8). This qualitatively matches the behavior simulated
260 by almost all 50 ensemble members of the CESM2-LE (Fig. 6C) and some other CMIP6 models
261 (Fig. S7). In contrast, only a few ensemble members of the CESM2-BB simulate a similar increase
262 in negative sea ice area trend over the GFED period as seen in the observations, with no clear
263 coherent response across the full ensemble (Fig. 6D). This raises the question of a potential role of
264 BB emissions in the observed Arctic sea ice loss since the late 1990s. Notably, this is challenging

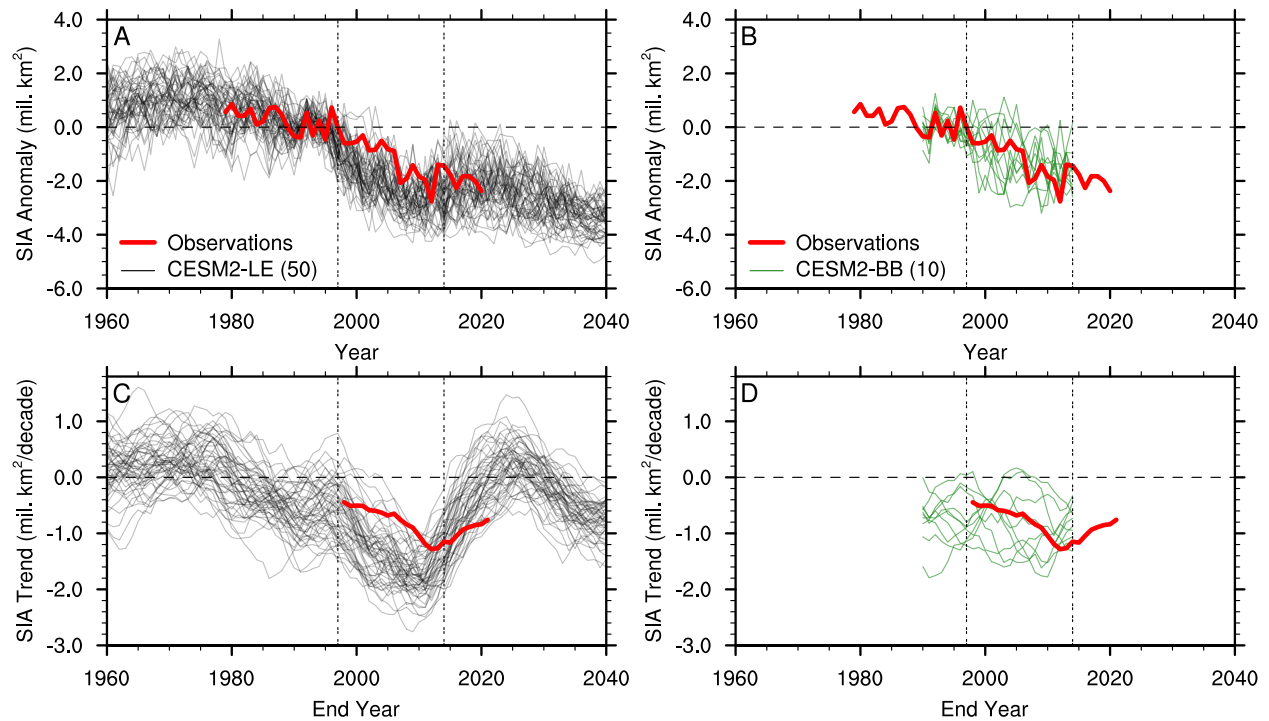


Fig. 6. Potential impact of BB emissions on observed Arctic sea ice decline. September sea ice area (SIA) (**A and B**) anomalies relative to the 1990–1996 average (when the two simulations share the same forcing) and (**C and D**) 20-year linear trends in each individual ensemble member of the (A and C) CESM2-LE and the (B and D) CESM2-BB (the ensemble size is indicated in parentheses in the legend) compared to observations. The horizontal dashed line indicates no anomalies in (A and B) and no trend in (C and D), and the two vertical double-dashed lines indicate the GFED period. In (C and D), values on the x-axis indicate the end year of the 20-year period over which the linear trend is computed.

265 to diagnose given the limitations of pre-GFED BB emission observations and the significant role
 266 of internal variability on Arctic sea ice trends (6, 7, 8, 44). Indeed, when taking into account
 267 internal variability by comparing the observations to all individual ensemble members, we cannot
 268 say that the observed Arctic sea ice decline since the late 1990s is different from the CESM2-LE
 269 or the CESM2-BB (Fig. 6, A and B). However, our results using the CESM2 indicate that BB
 270 emission variability strongly influences simulated multi-decadal Arctic sea ice trends. This should
 271 be further investigated in light of the observed record and is especially timely given the record
 272 Arctic fire years in 2019 and 2020 (15, 16, 17), the recent observed positive trend in burned area
 273 and severity of NH wildfires (48, 49, 50), and the projected increase in wildfires in the future
 274 (51, 52, 53).

275 **Materials and Methods**

276 **Observational data**

277 Observed estimates of NH monthly sea ice area since the beginning of the continuous satellite
278 record in 1979 are from the National Snow and Ice Data Center (NSIDC) Sea Ice Index version
279 3 (54), with the observational pole hole filled assuming sea ice concentration of 100%. Historical
280 anthropogenic CO₂ emissions are taken from the historical budget of the Global Carbon Project
281 (55). For global mean surface temperature, we use estimates from GISTemp v4 (56, 57) and
282 calculate anomalies relative to the period 1850–1900.

283 **CESM simulations**

284 The CESM Large Ensemble (CESM1-LE) (23) is a 40-member ensemble of the CESM1.1 model
285 (58) that has been widely used for Arctic sea ice studies and generally performs well when com-
286 pared to observations (43, 59, 60, 61, 62, 63). Historical simulations span 1920 to 2005, while the
287 RCP8.5 scenario simulations cover 2006 to 2100. The CESM1-LE uses the Community Atmo-
288 sphere Model version 5 (CAM5) (58) along with a 3-mode version of the Modal Aerosol Module
289 (MAM3) (64), and cloud-aerosol interactions are represented by the MG1 cloud microphysics
290 scheme (65).

291 With several science and infrastructure improvements, the CESM2 model (66) is the latest
292 generation of the CESM and NCAR’s contribution to CMIP6. Specifically, aerosols are simulated
293 through the use of the MAM4 approach (67) and cloud-aerosol interactions are represented by the
294 updated Morrison and Gettelman scheme (MG2) (68). The CAM5 shallow convection, planetary
295 boundary layer and cloud macrophysics schemes are replaced in CESM2 with an unified turbu-
296 lence scheme, the Cloud Layers Unified By Binormals (CLUBB) (69). As a result of these im-
297 provements, the CESM2 shows large reductions in low-latitude precipitation and short-wave cloud
298 radiative forcing biases, leading to improved historical simulations with respect to available obser-
299 vations compared to its previous major release, the CESM1.1 used in the CESM1-LE (66). Two

300 separate CESM2 configurations have been contributed to the CMIP6 effort, differing only in their
301 atmosphere component: the “low-top” (40 km, with limited chemistry) Community Atmosphere
302 Model version 6 (CAM6; referred to as CESM2) (66) and the “high-top” (140 km, with interactive
303 chemistry) Whole Atmosphere Community Climate Model version 6 (WACCM6; referred to as
304 CESM2-WACCM) (70). Previous analysis has shown that the low-top CESM2 simulates a thin-
305 ner 20th century sea ice cover than the high-top CESM2-WACCM (71) and the CESM1-LE (24).
306 Most of the analysis presented here focuses on a recently released large initial-condition ensemble
307 (referred to as CESM2-LE) that uses the version of the CESM2 with CAM6 as the atmosphere
308 component (22), but results from the CESM2-WACCM are also included in the comparison with
309 other CMIP6 models (Figs. S6 and S7).

310 The CESM2-LE (22) is a 100-member large ensemble suite that was run from 1850 to 2014
311 under historical forcing and from 2015 to 2100 following the medium-to-high SSP3-7.0 scenario
312 (72). The CESM2-LE initialization procedure was designed to include a mix of macro- and micro-
313 perturbations, where macro-perturbations were initialized from 20 independent restart files at 10-
314 year intervals (total of 20 ensemble members) and micro-initializations involved a small random
315 perturbation in 20 members for 4 different start years of the pre-industrial control simulation meant
316 to represent different AMOC states (total of 80 ensemble members). Note that most of this study
317 focuses on the first 50 members of the CESM2-LE since those follow CMIP6 protocols in terms
318 of BB emissions (19). For the second set of 50 members, the CMIP6 global BB emissions of all
319 relevant species were smoothed in time from 1990–2020 to remove inter-annual variability based
320 on the climate impacts of the high BB variability over the GFED period, as presented in this paper
321 and a companion paper (28).

322 **CESM2 sensitivity experiments with homogenized forcing**

323 To investigate the impact of the increased inter-annual variability in BB emissions over the GFED
324 period, we ran a set of sensitivity experiments using the CESM2 (referred to as CESM2-BB) in
325 which we averaged BB emissions from 1997–2014, computed on a monthly basis, such that BB

326 emissions have a fixed annual cycle while keeping the same integrated amount of emissions over
327 that same period. This approach is identical in nature to what was used in CMIP5 (21) and removes
328 any sharp transition with BB emissions over pre-GFED years as well as with the SSP BB emissions
329 since those are homogenized to the averaged GFED emissions. The CESM2-BB simulations are
330 initialized in 1990 from the first 10 members of the CESM2 and only BB emissions over the 40–
331 70°N latitudinal band from 1997–2014 are modified. This region is chosen to target BB emissions
332 from NH mid-latitude wildfires, but similar results are found by removing the variability in BB
333 emissions globally instead of only between 40–70°N (not shown), which highlights the impact of
334 NH mid-latitudes fires on Arctic climate. These sensitivity simulations are the same as the first 10
335 members used in a companion paper (28).

336 Although the ensemble size of the CESM2-BB is much smaller compared to the CESM2-LE,
337 we find that 10 ensemble members are enough to detect a forced response to the homogenized BB
338 emissions in the CESM2. Specifically, we compare the first 50 members of the CESM2-LE to
339 the last 50 members (Fig. S2, A and B), which also use homogenized BB emissions to avoid the
340 increase in BB variability over the GFED era (22). With 10 ensemble members, we are able to
341 detect a forced response that is statistically different in 2001 and from 2007–2011 for the September
342 sea ice area and from 2009–2011 and 2025–2027 for the 20-year linear trend in September
343 sea ice area (Fig. S2, C and D). Note, however, that for the last 50 members of the CESM2-LE
344 the chosen smoothing technique and years over which the smoothing is applied differ from what
345 we used in the CESM2-BB experiment. In particular, the smoothing in the CESM2-LE is applied
346 globally over 1990–2020 using an 11-year running mean filter, such that the integrated amount of
347 emissions over the GFED period is not the same as in the CMIP6 forcing (or the CESM2-BB).
348 Nonetheless, the Arctic sea ice response to homogenized BB forcing is similar between the last 50
349 members of the CESM2-LE and the CESM2-BB.

350 **CMIP6 simulations**

351 We also use simulations from a subset of CMIP6 models that provided at least three ensemble
352 members for the historical and SSP3-7.0 scenario simulations. As of December 2nd 2020, the
353 models that met this criteria (excluding the CESM2 and CESM2-WACCM described above) are:
354 ACCESS-CM2 (73, 74), ACCESS-ESM1.5 (75, 76), BCC-ESM1 (77, 78), CanESM5 (79, 80),
355 EC-Earth3-Veg (81, 82), FGOALS-g3 (83, 84), IPSL-CM6A-LR (85, 86), MIROC6 (87, 88),
356 MPI-ESM1.2-HR (89, 90), MPI-ESM1.2-LR (91, 92), MRI-ESM2.0 (93, 94) and NorESM2-LM
357 (95, 96). In cases where the ScenarioMIP SSP3-7.0 simulation was not available, we then used the
358 AerChemMIP SSP3-7.0 simulation that uses the same forcing as the ScenarioMIP SSP3-7.0 but
359 only extends to the end of 2055 (97). Even if a modeling center provided more than three ensemble
360 members, only the first three are used to allow for a consistent comparison across all CMIP6 mod-
361 els. Although using only CMIP6 models that provide at least three ensemble members limits the
362 total number of CMIP6 models included in our analysis, it is necessary to choose an ensemble size
363 that is large enough to represent the forced sea ice response to BB emissions, as some individual
364 members of the CESM2-LE show different trajectories despite the identified forced response to
365 the BB forcing (Fig. 6A). Using an ensemble size of three members was chosen as a compromise
366 since the ensemble mean of the first three ensemble members of the CESM2-LE match the full
367 ensemble mean reasonably well while requiring more members would further reduce the number
368 of available CMIP6 models.

369 **Criteria for determining sensitive versus not sensitive CMIP6 models**

370 The CMIP6 models are separated into a sensitive and a not sensitive category based on whether they
371 exhibit a similar sensitivity to the increased variability in BB emissions as the CESM2 (Figs. S6
372 and S7). First, we calculate 20-year linear trends in September sea ice area for each model, and
373 compare the slope of the 20-year linear trends between the reference period of end years 1978–
374 1990 and the acceleration period of end years 1997–2009. Note that we chose the last year of the
375 acceleration period to be 2009 instead of the last year of the GFED era (i.e., 2014) based on when

376 the CESM2-LE and CESM2-WACCM reach their maximum negative September sea ice area trend
377 (see Fig. S7). For a model to be characterized as sensitive, the slope of sea ice area trends over
378 the acceleration period needs to be at least 2 times larger (in absolute value) than the slope of sea
379 ice area trends over the reference period. This criteria is defined based on the relative increase
380 in sea ice trend for each model to account for the different magnitudes of sea ice loss across all
381 CMIP6 models (Fig. S7). We decided to choose two periods of same length and to exclude the
382 years 1991–1996 from the reference period because of the Mount Pinatubo volcanic eruption in
383 1991 and the global cooling that followed for a few years, which resulted in a peak increase in
384 Arctic sea ice extent about a year and a half after the eruption in some models (98). Note that the
385 classification into the sensitive and not sensitive category is not affected by the choice of reference
386 period or the exact magnitude of the accelerated sea ice loss.

387 **References**

- 388 [1] J. Stroeve, D. Notz, Changing state of Arctic sea ice across all seasons. *Environmental Re-*
389 *search Letters* **13**, 103001 (2018).
- 390 [2] R. Kwok, Arctic sea ice thickness, volume, and multiyear ice coverage: losses and coupled
391 variability (1958–2018). *Environmental Research Letters* **13**, 105005 (2018).
- 392 [3] D. Perovich, W. Meier, M. Tschudi, S. Hendricks, A. A. Petty, D. Divine, S. Farrell, S. Ger-
393 land, C. Haas, L. Kaleschke, O. Pavlova, R. Ricker, X. Tian-Kunze, M. Webster, K. Wood,
394 Sea ice. *Arctic Report Card 2020*, R. L. Thoman, J. Richter-Menge, M. L. Druckenmiller,
395 eds. (NOAA, 2020).
- 396 [4] I. Baxter, Q. Ding, A. Schweiger, M. L’Heureux, S. Baxter, T. Wang, Q. Zhang, K. Harnos,
397 B. Markle, D. Topal, *et al.*, How tropical Pacific surface cooling contributed to accelerated
398 sea ice melt from 2007 to 2012 as ice is thinned by anthropogenic forcing. *Journal of Climate*
399 **32**, 8583–8602 (2019).

- 400 [5] M. M. Holland, C. M. Bitz, B. Tremblay, Future abrupt reductions in the summer Arctic sea
401 ice. *Geophysical research letters* **33** (2006).
- 402 [6] J. E. Kay, M. M. Holland, A. Jahn, Inter-annual to multi-decadal Arctic sea ice extent trends
403 in a warming world. *Geophysical Research Letters* **38** (2011).
- 404 [7] J. J. Day, J. Hargreaves, J. Annan, A. Abe-Ouchi, Sources of multi-decadal variability in
405 Arctic sea ice extent. *Environmental Research Letters* **7**, 034011 (2012).
- 406 [8] N. C. Swart, J. C. Fyfe, E. Hawkins, J. E. Kay, A. Jahn, Influence of internal variability on
407 Arctic sea-ice trends. *Nature Climate Change* **5**, 86 (2015).
- 408 [9] L. M. Polvani, M. Previdi, M. R. England, G. Chiodo, K. L. Smith, Substantial twentieth-
409 century Arctic warming caused by ozone-depleting substances. *Nature Climate Change* **10**,
410 130–133 (2020).
- 411 [10] D. Shindell, G. Faluvegi, Climate response to regional radiative forcing during the twentieth
412 century. *Nature Geoscience* **2**, 294–300 (2009).
- 413 [11] T. J. Breider, L. J. Mickley, D. J. Jacob, C. Ge, J. Wang, M. Payer Sulprizio, B. Croft, D. A.
414 Ridley, J. R. McConnell, S. Sharma, *et al.*, Multidecadal trends in aerosol radiative forcing
415 over the Arctic: Contribution of changes in anthropogenic aerosol to Arctic warming since
416 1980. *Journal of Geophysical Research: Atmospheres* **122**, 3573–3594 (2017).
- 417 [12] L. Ren, Y. Yang, H. Wang, R. Zhang, P. Wang, H. Liao, Source attribution of Arctic black
418 carbon and sulfate aerosols and associated Arctic surface warming during 1980–2018. *Atmo-
419 spheric Chemistry and Physics* **20**, 9067–9085 (2020).
- 420 [13] L. Schmeisser, J. Backman, J. A. Ogren, E. Andrews, E. Asmi, S. Starkweather, T. Uttal,
421 M. Fiebig, S. Sharma, K. Eleftheriadis, *et al.*, Seasonality of aerosol optical properties in the
422 Arctic. *Atmospheric Chemistry and Physics* **18**, 11599–11622 (2018).

- 423 [14] J. Schmale, P. Zieger, A. M. Ekman, Aerosols in current and future Arctic climate. *Nature*
424 *Climate Change* **11**, 95–105 (2021).
- 425 [15] CAMS monitors unprecedented wildfires in the Arctic. *Copernicus Atmosphere*
426 *Monitoring Service* (11 July 2019). [https://atmosphere.copernicus.eu/
427 cams-monitors-unprecedented-wildfires-arctic](https://atmosphere.copernicus.eu/cams-monitors-unprecedented-wildfires-arctic).
- 428 [16] Another active year for Arctic wildfires. *Copernicus Atmosphere Mon-*
429 *itoring Service* (8 July 2020). [https://atmosphere.copernicus.eu/
430 another-active-year-arctic-wildfires](https://atmosphere.copernicus.eu/another-active-year-arctic-wildfires).
- 431 [17] A. Witze, The arctic is burning like never before — and that’s bad news for climate change.
432 *Nature* **585**, 336–337 (2020).
- 433 [18] Y. Zou, P. J. Rasch, H. Wang, Z. Xie, R. Zhang, Increasing large wildfires over the western
434 United States linked to diminishing sea ice in the Arctic. *Nature Communications* **12** (2021).
- 435 [19] M. J. Van Marle, S. Kloster, B. I. Magi, J. R. Marlon, A.-L. Daniau, R. D. Field, A. Arneth,
436 M. Forrest, S. Hantson, N. M. Kehrwald, *et al.*, Historic global biomass burning emissions
437 for CMIP6 (BB4CMIP) based on merging satellite observations with proxies and fire models
438 (1750–2015). *Geoscientific Model Development* **10**, 3329–3357 (2017).
- 439 [20] G. R. Van Der Werf, J. T. Randerson, L. Giglio, T. T. Van Leeuwen, Y. Chen, B. M. Rogers,
440 M. Mu, M. J. Van Marle, D. C. Morton, G. J. Collatz, *et al.*, Global fire emissions estimates
441 during 1997–2016. *Earth System Science Data* **9**, 697–720 (2017).
- 442 [21] J.-F. Lamarque, T. C. Bond, V. Eyring, C. Granier, A. Heil, Z. Klimont, D. Lee, C. Liousse,
443 A. Mieville, B. Owen, *et al.*, Historical (1850–2000) gridded anthropogenic and biomass
444 burning emissions of reactive gases and aerosols: methodology and application. *Atmospheric*
445 *Chemistry and Physics* **10**, 7017–7039 (2010).

- 446 [22] K. B. Rodgers, S.-S. Lee, N. Rosenbloom, A. Timmermann, G. Danabasoglu, C. Deser, J. Ed-
447 wards, J.-E. Kim, I. R. Simpson, K. Stein, *et al.*, Ubiquity of human-induced changes in
448 climate variability. *Earth System Dynamics* **12**, 1393–1411 (2021).
- 449 [23] J. E. Kay, C. Deser, A. Phillips, A. Mai, C. Hannay, G. Strand, J. M. Arblaster, S. Bates,
450 G. Danabasoglu, J. Edwards, *et al.*, The Community Earth System Model (CESM) large
451 ensemble project: A community resource for studying climate change in the presence of
452 internal climate variability. *Bulletin of the American Meteorological Society* **96**, 1333–1349
453 (2015).
- 454 [24] P. DeRepentigny, A. Jahn, M. M. Holland, A. Smith, Arctic sea ice in two configurations of
455 the CESM2 during the 20th and 21st centuries. *Journal of Geophysical Research: Oceans*
456 **125**, e2020JC016133 (2020).
- 457 [25] A. Jahn, Reduced probability of ice-free summers for 1.5°C compared to 2°C warming. *Nature*
458 *Climate Change* **8**, 409–413 (2018).
- 459 [26] B. D. Santer, C. Bonfils, J. F. Painter, M. D. Zelinka, C. Mears, S. Solomon, G. A. Schmidt,
460 J. C. Fyfe, J. N. Cole, L. Nazarenko, *et al.*, Volcanic contribution to decadal changes in
461 tropospheric temperature. *Nature Geoscience* **7**, 185–189 (2014).
- 462 [27] G. A. Schmidt, D. T. Shindell, K. Tsigaridis, Reconciling warming trends. *Nature Geoscience*
463 **7**, 158–160 (2014).
- 464 [28] J. T. Fasullo, J.-F. Lamarque, C. Hannay, N. Rosenbloom, S. Tilmes, P. DeRepentigny,
465 A. Jahn, C. Deser, Spurious Late Historical-Era Warming in CESM2 Driven by Prescribed
466 Biomass Burning Emissions. *Geophysical Research Letters* **49**, e2021GL097420 (2022).
- 467 [29] L. Fierce, N. Riemer, T. C. Bond, Explaining variance in black carbon’s aging timescale.
468 *Atmospheric Chemistry and Physics* **15**, 3173–3191 (2015).

- 469 [30] X. Li, A. H. Lynch, D. A. Bailey, S. R. Stephenson, S. Veland, The impact of black carbon
470 emissions from projected Arctic shipping on regional ice transport. *Climate Dynamics* pp.
471 1–14 (2021).
- 472 [31] M. Ramana, A. Devi, CCN concentrations and BC warming influenced by maritime ship
473 emitted aerosol plumes over southern Bay of Bengal. *Scientific reports* **6**, 1–8 (2016).
- 474 [32] K. Carslaw, L. Lee, C. Reddington, K. Pringle, A. Rap, P. Forster, G. Mann, D. Spracklen,
475 M. Woodhouse, L. Regayre, *et al.*, Large contribution of natural aerosols to uncertainty in
476 indirect forcing. *Nature* **503**, 67–71 (2013).
- 477 [33] S. Twomey, The influence of pollution on the shortwave albedo of clouds. *Journal of the*
478 *atmospheric sciences* **34**, 1149–1152 (1977).
- 479 [34] T. Mauritsen, J. Sedlar, M. Tjernström, C. Leck, M. Martin, M. Shupe, S. Sjogren, B. Sierau,
480 P. Persson, I. Brooks, *et al.*, An Arctic CCN-limited cloud-aerosol regime. *Atmospheric*
481 *Chemistry and Physics* **11**, 165–173 (2011).
- 482 [35] M. Winton, Do climate models underestimate the sensitivity of Northern Hemisphere sea ice
483 cover? *Journal of Climate* **24**, 3924–3934 (2011).
- 484 [36] I. Mahlstein, R. Knutti, September Arctic sea ice predicted to disappear near 2°C global
485 warming above present. *Journal of Geophysical Research: Atmospheres* **117** (2012).
- 486 [37] J. Stroeve, D. Notz, Insights on past and future sea-ice evolution from combining observations
487 and models. *Global and Planetary Change* **135**, 119–132 (2015).
- 488 [38] D. Notz, J. Stroeve, Observed Arctic sea-ice loss directly follows anthropogenic CO₂ emis-
489 sion. *Science* **354**, 747–750 (2016).
- 490 [39] A. L. Niederrenk, D. Notz, Arctic sea ice in a 1.5°C warmer world. *Geophysical Research*
491 *Letters* **45**, 1963–1971 (2018).

- 492 [40] E. Rosenblum, I. Eisenman, Sea ice trends in climate models only accurate in runs with
493 biased global warming. *Journal of Climate* **30**, 6265–6278 (2017).
- 494 [41] SIMIP Community, Arctic Sea Ice in CMIP6. *Geophysical Research Letters* **47**,
495 e2019GL086749 (2020).
- 496 [42] D. Notz, J. Marotzke, Observations reveal external driver for Arctic sea-ice retreat. *Geophys-*
497 *ical Research Letters* **39** (2012).
- 498 [43] M. England, A. Jahn, L. Polvani, Nonuniform Contribution of Internal Variability to Recent
499 Arctic Sea Ice Loss. *Journal of Climate* **32**, 4039–4053 (2019).
- 500 [44] Q. Ding, A. Schweiger, M. L’Heureux, E. J. Steig, D. S. Battisti, N. C. Johnson, E. Blanchard-
501 Wrigglesworth, S. Po-Chedley, Q. Zhang, K. Harnos, *et al.*, Fingerprints of internal drivers
502 of Arctic sea ice loss in observations and model simulations. *Nature Geoscience* **12**, 28–33
503 (2019).
- 504 [45] E. Rosenblum, I. Eisenman, Faster Arctic sea ice retreat in CMIP5 than in CMIP3 due to
505 volcanoes. *Journal of Climate* **29**, 9179–9188 (2016).
- 506 [46] J. C. Stroeve, M. C. Serreze, M. M. Holland, J. E. Kay, J. Malanik, A. P. Barrett, The Arc-
507 tic’s rapidly shrinking sea ice cover: a research synthesis. *Climatic change* **110**, 1005–1027
508 (2012).
- 509 [47] M. C. Serreze, J. Stroeve, Arctic sea ice trends, variability and implications for seasonal ice
510 forecasting. *Philosophical Transactions of the Royal Society A: Mathematical, Physical and*
511 *Engineering Sciences* **373**, 20140159 (2015).
- 512 [48] R. Kelly, M. L. Chipman, P. E. Higuera, I. Stefanova, L. B. Brubaker, F. S. Hu, Recent
513 burning of boreal forests exceeds fire regime limits of the past 10,000 years. *Proceedings of*
514 *the National Academy of Sciences* **110**, 13055–13060 (2013).

- 515 [49] C. C. Hanes, X. Wang, P. Jain, M.-A. Parisien, J. M. Little, M. D. Flannigan, Fire-regime
516 changes in Canada over the last half century. *Canadian Journal of Forest Research* **49**, 256–
517 269 (2019).
- 518 [50] Y. Huang, Y. Jin, M. W. Schwartz, J. H. Thorne, Intensified burn severity in California’s
519 northern coastal mountains by drier climatic condition. *Environmental Research Letters* **15**,
520 104033 (2020).
- 521 [51] W. J. de Groot, M. D. Flannigan, A. S. Cantin, Climate change impacts on future boreal fire
522 regimes. *Forest Ecology and Management* **294**, 35–44 (2013).
- 523 [52] B. Sherstyukov, A. Sherstyukov, Assessment of increase in forest fire risk in Russia till the
524 late 21st century based on scenario experiments with fifth-generation climate models. *Russian*
525 *Meteorology and Hydrology* **39**, 292–301 (2014).
- 526 [53] W. Tang, S. Tilmes, D. M. Lawrence, F. Li, C. He, L. K. Emmons, R. R. Buchholz, Wildfires
527 in the 21st Century under Different Shared Socioeconomic Pathways (SSPs) and Geoengi-
528 neering Scenarios in CESM2/WACCM6. *Earth’s Future* (2021). In review.
- 529 [54] F. Fetterer, K. Knowles, W. Meier, M. Savoie, A. Windnagel, Sea Ice Index, Version 3
530 [monthly values from 1979 to 2020], National Snow and Ice Data Center, Boulder, Colorado,
531 USA (2017). Accessed May 2020.
- 532 [55] Global Carbon Project, Supplemental data of Global Carbon Budget 2019 (Version 1.0),
533 Global Carbon Project (2019). <https://doi.org/10.18160/gcp-2019>.
- 534 [56] GISTEMP Team, GISS Surface Temperature Analysis (GISTEMP), version
535 4, NASA Goddard Institute for Space Studies (2021). Dataset accessed at
536 <https://data.giss.nasa.gov/gistemp/>.
- 537 [57] N. J. Lenssen, G. A. Schmidt, J. E. Hansen, M. J. Menne, A. Persin, R. Ruedy, D. Zyss,

- 538 Improvements in the GISTEMP uncertainty model. *Journal of Geophysical Research: Atmo-*
539 *spheres* **124**, 6307–6326 (2019).
- 540 [58] J. W. Hurrell, M. M. Holland, P. R. Gent, S. Ghan, J. E. Kay, P. J. Kushner, J.-F. Lamarque,
541 W. G. Large, D. Lawrence, K. Lindsay, *et al.*, The Community Earth System Model: A
542 Framework for Collaborative Research. *Bulletin of the American Meteorological Society* **94**,
543 1339–1360 (2013).
- 544 [59] A. Jahn, J. E. Kay, M. M. Holland, D. M. Hall, How predictable is the timing of a summer
545 ice-free Arctic? *Geophysical Research Letters* **43**, 9113–9120 (2016).
- 546 [60] K. R. Barnhart, C. R. Miller, I. Overeem, J. E. Kay, Mapping the future expansion of Arctic
547 open water. *Nature Climate Change* **6**, 280 (2016).
- 548 [61] P. DeRepentigny, L. B. Tremblay, R. Newton, S. Pfirman, Patterns of sea ice retreat in the
549 transition to a seasonally ice-free Arctic. *Journal of Climate* **29**, 6993–7008 (2016).
- 550 [62] M. C. Kirchmeier-Young, F. W. Zwiers, N. P. Gillett, Attribution of extreme events in Arctic
551 sea ice extent. *Journal of Climate* **30**, 553–571 (2017).
- 552 [63] A. Smith, A. Jahn, Definition differences and internal variability affect the simulated Arctic
553 sea ice melt season. *The Cryosphere* **13**, 1–20 (2019).
- 554 [64] X. Liu, R. C. Easter, S. J. Ghan, R. Zaveri, P. Rasch, X. Shi, J.-F. Lamarque, A. Gettelman,
555 H. Morrison, F. Vitt, *et al.*, Toward a minimal representation of aerosols in climate mod-
556 els: Description and evaluation in the Community Atmosphere Model CAM5. *Geoscientific*
557 *Model Development* **5**, 709–739 (2012).
- 558 [65] H. Morrison, A. Gettelman, A new two-moment bulk stratiform cloud microphysics scheme
559 in the Community Atmosphere Model, version 3 (CAM3). Part I: Description and numerical
560 tests. *Journal of Climate* **21**, 3642–3659 (2008).

- 561 [66] G. Danabasoglu, J.-F. Lamarque, J. Bacmeister, D. Bailey, A. DuVivier, J. Edwards, L. Em-
562 mons, J. Fasullo, R. Garcia, A. Gettelman, *et al.*, The Community Earth System Model Ver-
563 sion 2 (CESM2). *Journal of Advances in Modeling Earth Systems* **12**, e2019MS001916
564 (2020).
- 565 [67] X. Liu, P.-L. Ma, H. Wang, S. Tilmes, B. Singh, R. Easter, S. Ghan, P. Rasch, Description
566 and evaluation of a new four-mode version of the Modal Aerosol Module (MAM4) within
567 version 5.3 of the Community Atmosphere Model. *Geoscientific Model Development* **9**, 505–
568 522 (2016).
- 569 [68] A. Gettelman, H. Morrison, Advanced two-moment bulk microphysics for global models.
570 Part I: Off-line tests and comparison with other schemes. *Journal of Climate* **28**, 1268–1287
571 (2015).
- 572 [69] P. A. Bogenschutz, A. Gettelman, H. Morrison, V. E. Larson, C. Craig, D. P. Schanen, Higher-
573 order turbulence closure and its impact on climate simulations in the Community Atmosphere
574 Model. *Journal of Climate* **26**, 9655–9676 (2013).
- 575 [70] A. Gettelman, M. Mills, D. Kinnison, R. Garcia, A. Smith, D. Marsh, S. Tilmes, F. Vitt,
576 C. Bardeen, J. McInerney, *et al.*, The Whole Atmosphere Community Climate Model Version
577 6 (WACCM6). *Journal of Geophysical Research: Atmospheres* (2019).
- 578 [71] A. K. DuVivier, M. M. Holland, J. E. Kay, S. Tilmes, A. Gettelman, D. A. Bailey, Arc-
579 tic and Antarctic sea ice mean state in the Community Earth System Model version 2 and
580 the influence of atmospheric chemistry. *Journal of Geophysical Research: Oceans* **125**,
581 e2019JC015934 (2020).
- 582 [72] B. C. O’Neill, C. Tebaldi, D. P. v. Vuuren, V. Eyring, P. Friedlingstein, G. Hurtt, R. Knutti,
583 E. Kriegler, J.-F. Lamarque, J. Lowe, *et al.*, The scenario model intercomparison project
584 (ScenarioMIP) for CMIP6. *Geoscientific Model Development* **9**, 3461–3482 (2016).

- 585 [73] M. Dix, D. Bi, P. Dobrohotoff, R. Fiedler, I. Harman, R. Law, C. Mackallah, S. Marsland,
586 S. O’Farrell, H. Rashid, J. Srbinovsky, A. Sullivan, C. Trenham, P. Vohralik, I. Watterson,
587 G. Williams, M. Woodhouse, R. Bodman, F. B. Dias, C. Domingues, N. Hannah, A. Heerde-
588 gen, A. Savita, S. Wales, C. Allen, K. Druken, B. Evans, C. Richards, S. M. Ridzwan,
589 D. Roberts, J. Smillie, K. Snow, M. Ward, R. Yang, CSIRO-ARCCSS ACCESS-CM2 model
590 output prepared for CMIP6 CMIP historical (2019). Version 20200817.
- 591 [74] M. Dix, D. Bi, P. Dobrohotoff, R. Fiedler, I. Harman, R. Law, C. Mackallah, S. Marsland,
592 S. O’Farrell, H. Rashid, J. Srbinovsky, A. Sullivan, C. Trenham, P. Vohralik, I. Watterson,
593 G. Williams, M. Woodhouse, R. Bodman, F. B. Dias, C. Domingues, N. Hannah, A. Heerde-
594 gen, A. Savita, S. Wales, C. Allen, K. Druken, B. Evans, C. Richards, S. M. Ridzwan,
595 D. Roberts, J. Smillie, K. Snow, M. Ward, R. Yang, CSIRO-ARCCSS ACCESS-CM2 model
596 output prepared for CMIP6 ScenarioMIP ssp370 (2019). Version 20200817.
- 597 [75] T. Ziehn, M. Chamberlain, A. Lenton, R. Law, R. Bodman, M. Dix, Y. Wang, P. Dobrohotoff,
598 J. Srbinovsky, L. Stevens, P. Vohralik, C. Mackallah, A. Sullivan, S. O’Farrell, K. Druken,
599 CSIRO ACCESS-ESM1.5 model output prepared for CMIP6 CMIP historical (2019). Version
600 20200817.
- 601 [76] T. Ziehn, M. Chamberlain, A. Lenton, R. Law, R. Bodman, M. Dix, Y. Wang, P. Dobrohotoff,
602 J. Srbinovsky, L. Stevens, P. Vohralik, C. Mackallah, A. Sullivan, S. O’Farrell, K. Druken,
603 CSIRO ACCESS-ESM1.5 model output prepared for CMIP6 ScenarioMIP ssp370 (2019).
604 Version 20200817.
- 605 [77] J. Zhang, T. Wu, X. Shi, F. Zhang, J. Li, M. Chu, Q. Liu, J. Yan, Q. Ma, M. Wei, BCC
606 BCC-ESM1 model output prepared for CMIP6 CMIP historical (2018). Version 20200218.
- 607 [78] J. Zhang, T. Wu, X. Shi, F. Zhang, J. Li, M. Chu, Q. Liu, J. Yan, Q. Ma, M. Wei, BCC BCC-
608 ESM1 model output prepared for CMIP6 AerChemMIP ssp370 (2019). Version 20200219.
- 609 [79] N. C. Swart, J. N. Cole, V. V. Kharin, M. Lazare, J. F. Scinocca, N. P. Gillett, J. Anstey,

- 610 V. Arora, J. R. Christian, Y. Jiao, W. G. Lee, F. Majaess, O. A. Saenko, C. Seiler, C. Seinen,
611 A. Shao, L. Solheim, K. von Salzen, D. Yang, B. Winter, M. Sigmond, CCCma CanESM5
612 model output prepared for CMIP6 CMIP historical (2019). Version 20190429.
- 613 [80] N. C. Swart, J. N. Cole, V. V. Kharin, M. Lazare, J. F. Scinocca, N. P. Gillett, J. Anstey,
614 V. Arora, J. R. Christian, Y. Jiao, W. G. Lee, F. Majaess, O. A. Saenko, C. Seiler, C. Seinen,
615 A. Shao, L. Solheim, K. von Salzen, D. Yang, B. Winter, M. Sigmond, CCCma CanESM5
616 model output prepared for CMIP6 ScenarioMIP ssp370 (2019). Version 20190429.
- 617 [81] EC-Earth Consortium (EC-Earth), EC-Earth-Consortium EC-Earth3-Veg model output pre-
618 pared for CMIP6 CMIP historical (2019). Version 20200919.
- 619 [82] EC-Earth Consortium (EC-Earth), EC-Earth-Consortium EC-Earth3-Veg model output pre-
620 pared for CMIP6 ScenarioMIP ssp370 (2019). Version 20200919.
- 621 [83] L. Li, CAS FGOALS-g3 model output prepared for CMIP6 CMIP historical (2019). Version
622 20191029.
- 623 [84] L. Li, CAS FGOALS-g3 model output prepared for CMIP6 ScenarioMIP ssp370 (2019).
624 Version 20191029.
- 625 [85] O. Boucher, S. Denvil, G. Levvasseur, A. Cozic, A. Caubel, M.-A. Foujols, Y. Meurdesoif,
626 P. Cadule, M. Devilliers, J. Ghattas, N. Lebas, T. Lurton, L. Mellul, I. Musat, J. Mignot,
627 F. Cheruy, IPSL IPSL-CM6A-LR model output prepared for CMIP6 CMIP historical (2018).
628 Version 20180803.
- 629 [86] O. Boucher, S. Denvil, G. Levvasseur, A. Cozic, A. Caubel, M.-A. Foujols, Y. Meurdesoif,
630 P. Cadule, M. Devilliers, E. Dupont, T. Lurton, IPSL IPSL-CM6A-LR model output prepared
631 for CMIP6 ScenarioMIP ssp370 (2019). Version 20190119.
- 632 [87] H. Tatebe, M. Watanabe, MIROC MIROC6 model output prepared for CMIP6 CMIP histor-
633 ical (2018). Version 20181212.

- 634 [88] H. Shiogama, M. Abe, H. Tatebe, MIROC MIROC6 model output prepared for CMIP6 Sce-
635 narioMIP ssp370 (2019). Version 20190627.
- 636 [89] J. Jungclaus, M. Bittner, K.-H. Wieners, F. Wachsman, M. Schupfner, S. Legutke, M. Gior-
637 getta, C. Reick, V. Gayler, H. Haak, P. de Vrese, T. Raddatz, M. Esch, T. Mauritsen, J.-S.
638 von Storch, J. Behrens, V. Brovkin, M. Claussen, T. Crueger, I. Fast, S. Fiedler, S. Hage-
639 mann, C. Hohenegger, T. Jahns, S. Kloster, S. Kinne, G. Lasslop, L. Kornblueh, J. Marotzke,
640 D. Matei, K. Meraner, U. Mikolajewicz, K. Modali, W. Müller, J. Nabel, D. Notz, K. Pe-
641 ters, R. Pincus, H. Pohlmann, J. Pongratz, S. Rast, H. Schmidt, R. Schnur, U. Schulzweida,
642 K. Six, B. Stevens, A. Voigt, E. Roeckner, MPI-M MPI-ESM1.2-HR model output prepared
643 for CMIP6 CMIP historical (2019). Version 20190710.
- 644 [90] M. Schupfner, *et al.*, DKRZ MPI-ESM1.2-HR model output prepared for CMIP6 Scenari-
645 oMIP ssp370 (2019). Version 20190815.
- 646 [91] K.-H. Wieners, M. Giorgetta, J. Jungclaus, C. Reick, M. Esch, M. Bittner, S. Legutke,
647 M. Schupfner, F. Wachsman, V. Gayler, H. Haak, P. de Vrese, T. Raddatz, T. Mauritsen,
648 J.-S. von Storch, J. Behrens, V. Brovkin, M. Claussen, T. Crueger, I. Fast, S. Fiedler, S. Hage-
649 mann, C. Hohenegger, T. Jahns, S. Kloster, S. Kinne, G. Lasslop, L. Kornblueh, J. Marotzke,
650 D. Matei, K. Meraner, U. Mikolajewicz, K. Modali, W. Müller, J. Nabel, D. Notz, K. Pe-
651 ters, R. Pincus, H. Pohlmann, J. Pongratz, S. Rast, H. Schmidt, R. Schnur, U. Schulzweida,
652 K. Six, B. Stevens, A. Voigt, E. Roeckner, MPI-M MPI-ESM1.2-LR model output prepared
653 for CMIP6 CMIP historical (2019). Version 20190710.
- 654 [92] K.-H. Wieners, M. Giorgetta, J. Jungclaus, C. Reick, M. Esch, M. Bittner, V. Gayler, H. Haak,
655 P. de Vrese, T. Raddatz, T. Mauritsen, J.-S. von Storch, J. Behrens, V. Brovkin, M. Claussen,
656 T. Crueger, I. Fast, S. Fiedler, S. Hagemann, C. Hohenegger, T. Jahns, S. Kloster, S. Kinne,
657 G. Lasslop, L. Kornblueh, J. Marotzke, D. Matei, K. Meraner, U. Mikolajewicz, K. Modali,
658 W. Müller, J. Nabel, D. Notz, K. Peters, R. Pincus, H. Pohlmann, J. Pongratz, S. Rast,
659 H. Schmidt, R. Schnur, U. Schulzweida, K. Six, B. Stevens, A. Voigt, E. Roeckner, MPI-

660 M MPI-ESM1.2-LR model output prepared for CMIP6 ScenarioMIP ssp370 (2019). Version
661 20190710.

662 [93] S. Yukimoto, T. Koshiro, H. Kawai, N. Oshima, K. Yoshida, S. Urakawa, H. Tsujino,
663 M. Deushi, T. Tanaka, M. Hosaka, H. Yoshimura, E. Shindo, R. Mizuta, M. Ishii, A. Obata,
664 Y. Adachi, MRI MRI-ESM2.0 model output prepared for CMIP6 CMIP historical (2019).
665 Version 20190904.

666 [94] S. Yukimoto, T. Koshiro, H. Kawai, N. Oshima, K. Yoshida, S. Urakawa, H. Tsujino,
667 M. Deushi, T. Tanaka, M. Hosaka, H. Yoshimura, E. Shindo, R. Mizuta, M. Ishii, A. Obata,
668 Y. Adachi, MRI MRI-ESM2.0 model output prepared for CMIP6 ScenarioMIP ssp370
669 (2019). Version 20190904.

670 [95] Ø. Seland, M. Bentsen, D. J. L. Olivière, T. Toniazzo, A. Gjermundsen, L. S. Graff, J. B.
671 Debernard, A. K. Gupta, Y. He, A. Kirkevåg, J. Schwinger, J. Tjiputra, K. S. Aas, I. Bethke,
672 Y. Fan, J. Griesfeller, A. Grini, C. Guo, M. Ilıcak, I. H. H. Karset, O. A. Landgren, J. Liakka,
673 K. O. Moseid, A. Nummelin, C. Spensberger, H. Tang, Z. Zhang, C. Heinze, T. Iversen,
674 M. Schulz, NCC NorESM2-LM model output prepared for CMIP6 CMIP historical (2019).
675 Version 20191108.

676 [96] Ø. Seland, M. Bentsen, D. J. L. Olivière, T. Toniazzo, A. Gjermundsen, L. S. Graff, J. B. De-
677 bernard, A. K. Gupta, Y. He, A. Kirkevåg, J. Schwinger, J. Tjiputra, K. S. Aas, I. Bethke,
678 Y. Fan, J. Griesfeller, A. Grini, C. Guo, M. Ilıcak, I. H. H. Karset, O. A. Landgren, J. Liakka,
679 K. O. Moseid, A. Nummelin, C. Spensberger, H. Tang, Z. Zhang, C. Heinze, T. Iversen,
680 M. Schulz, NCC NorESM2-LM model output prepared for CMIP6 ScenarioMIP ssp370
681 (2019). Version 20191108.

682 [97] W. J. Collins, J.-F. Lamarque, M. Schulz, O. Boucher, V. Eyring, M. I. Hegglin, A. Maycock,
683 G. Myhre, M. Prather, D. Shindell, *et al.*, AerChemMIP: quantifying the effects of chemistry
684 and aerosols in CMIP6. *Geoscientific Model Development* **10**, 585–607 (2017).

685 [98] M.-E. Gagné, M. Kirchmeier-Young, N. Gillett, J. Fyfe, Arctic sea ice response to the erup-
686 tions of Agung, El Chichón, and Pinatubo. *Journal of Geophysical Research: Atmospheres*
687 **122**, 8071–8078 (2017).

688 **Acknowledgments**

689 **Funding:** P. DeRepentigny is supported by the Natural Sciences and Engineering Council of
690 Canada (NSERC) and the Fonds de recherche du Québec – Nature et Technologies (FRQNT)
691 through PhD scholarships and by NSF-OPP CAREER award 1847398. Part of the revisions of
692 this manuscript were carried out while P. DeRepentigny was supported by NSF-AGS CAREER
693 award 1554659 and the Advanced Study Program of the National Center for Atmospheric Re-
694 search (NCAR). A. Jahn’s and A. Barrett’s contribution is supported by NSF-OPP CAREER award
695 1847398. Contributions from M. M. Holland, J.-F. Lamarque, C. Hannay, M. J. Mills, D. A. Bai-
696 ley and S. Tilmes are supported by NCAR, which is a major facility sponsored by the NSF under
697 Cooperative Agreement No. 1852977. J. E. Kay was supported by NSF-AGS CAREER award
698 1554659. The efforts of J. Fasullo were supported by NASA Award 80NSSC17K0565, by NSF
699 Award #AGS-1419571, and by the Regional and Global Model Analysis (RGMA) component of
700 the Earth and Environmental System Modeling Program of the U.S. Department of Energy’s Office
701 of Biological & Environmental Research (BER) via National Science Foundation IA 1844590.

702 The CESM project is supported primarily by the National Science Foundation (NSF). This ma-
703 terial is based upon work supported by NCAR, which is a major facility sponsored by the NSF
704 under Cooperative Agreement No. 1852977. Computing and data storage resources, including the
705 Yellowstone (<http://n2t.net/ark:/85065/d7wd3xhc>) and Cheyenne (doi:10.5065/D6RX99HX)
706 supercomputers, were provided by the Computational and Information Systems Laboratory (CISL)
707 at NCAR. We thank all the scientists, software engineers, and administrators who contributed to
708 the development of CESM and the CESM1 and CESM2 Large Ensemble Community Projects.
709 We also acknowledge supercomputing resources provided by the IBS Center for Climate Physics

710 in South Korea for the CESM2 Large Ensemble Project.

711 We acknowledge the World Climate Research Programme, which, through its Working Group
712 on Coupled Modelling, coordinated and promoted CMIP6. We thank the climate modeling groups
713 for producing and making available their model output, the Earth System Grid Federation (ESGF)
714 for archiving the data and providing access, and the multiple funding agencies who support CMIP6
715 and ESGF.

716 We also thank Alice DuVivier, Clara Deser, Walt N. Meier, Andrew Gettelman and Christina
717 S. McCluskey for useful discussions and three anonymous reviewers for valuable comments on
718 an earlier version of this manuscript. Data analysis and visualization were done using the NCAR
719 Command Language (<http://dx.doi.org/10.5065/D6WD3XH5>).

720

721 **Author contributions:** P. DeRepentigny and A. Jahn designed the study. P. DeRepentigny per-
722 formed the analysis and wrote the manuscript under the supervision of A. Jahn. M. M. Holland,
723 J. Fasullo and J.-F. Lamarque contributed to the experiment design and provided CESM specific
724 expertise. J. E. Kay provided valuable guidance on statistical analysis and cloud-aerosol-radiation
725 interactions. C. Hannay and P. DeRepentigny conducted the sensitivity simulations. M. J. Mills
726 and S. Tilmes provided aerosol emission expertise. D. A. Bailey provided valuable assistance for
727 conducting the sensitivity simulations. A. Barrett compiled CMIP6 data. All authors provided crit-
728 ical feedback and collaborated in shaping the research, analysis and final version of the manuscript.

729

730 **Competing interests:** The authors declare no competing interests.

731

732 **Data and materials availability:** Previous and current versions of the CESM are freely avail-
733 able at <https://www.cesm.ucar.edu/models/>. The CESM2-LE data analyzed in this study
734 can be accessed at [https://www.cesm.ucar.edu/projects/community-projects/LENS2/](https://www.cesm.ucar.edu/projects/community-projects/LENS2/data-sets.html)
735 [data-sets.html](https://www.cesm.ucar.edu/projects/community-projects/LENS2/data-sets.html). The CESM1-LE data can be found at [https://www.cesm.ucar.edu/projects/](https://www.cesm.ucar.edu/projects/community-projects/LENS/)
736 [community-projects/LENS/](https://www.cesm.ucar.edu/projects/community-projects/LENS/). Data from the CMIP6 models analyzed in this study are freely

737 available from the Earth System Grid Federation (ESGF) at esgf-node.llnl.gov/search/
738 [cmip6/](https://esgf-node.llnl.gov/search/cmip6/). The CESM2-BB sensitivity simulations are available on NCAR's Geoscience Data Ex-
739 change (GDEX) at https://gdex.ucar.edu/dataset/239_fasullo.html (doi:10.5065/7f7c-
740 zw94).

1 **Supplementary Materials**

2 **Enhanced simulated early 21st century Arctic sea ice loss due to CMIP6 biomass**
3 **burning emissions**

4 **Authors**

5 Patricia DeRepentigny^{1,2*†}, Alexandra Jahn^{1,2}, Marika M. Holland³, Jennifer E. Kay^{1,4}, John
6 Fasullo³, Jean-François Lamarque³, Simone Tilmes⁵, Cécile Hannay³, Michael J. Mills⁵, David
7 A. Bailey³, and Andrew Barrett⁶

8 **Affiliations**

9 ¹Department of Atmospheric and Oceanic Sciences, University of Colorado Boulder, Boulder, CO,
10 USA.

11 ²Institute of Arctic and Alpine Research, University of Colorado Boulder, Boulder, CO, USA.

12 ³Climate and Global Dynamics Laboratory, National Center for Atmospheric Research, Boulder,
13 CO, USA.

14 ⁴Cooperative Institute for Research in Environmental Sciences, University of Colorado Boulder,
15 Boulder, CO, USA.

16 ⁵Atmospheric Chemistry Observations and Modeling Laboratory, National Center for Atmospheric
17 Research, Boulder CO, USA.

18 ⁶National Snow and Ice Data Center, University of Colorado Boulder, Boulder, CO, USA.

19

20 *Corresponding author: Patricia DeRepentigny, patricia.derepentigny@colorado.edu

21

22 †Now at the Climate and Global Dynamics Laboratory, National Center for Atmospheric Research,
23 Boulder, CO, USA.

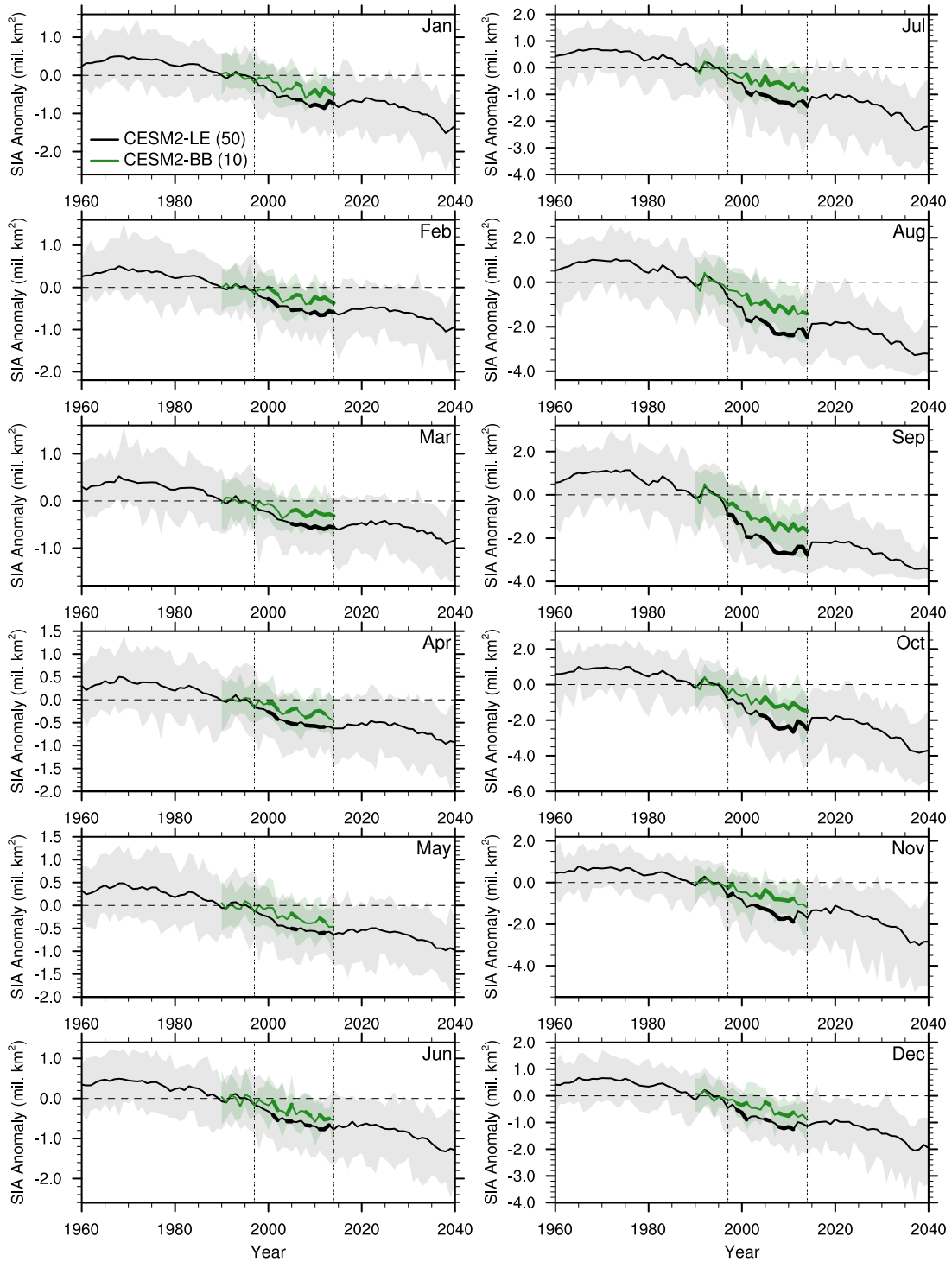


Fig. S1. BB emissions impact on Arctic sea ice in all months. Sea ice area (SIA) anomalies relative to the 1990–1996 average (when the two simulations share the same forcing) in each month of the year in the CESM2-LE and the CESM2-BB. The ensemble mean is shown by the solid line, the full ensemble range is shown by the shading, the horizontal dashed line indicates no anomalies, and the two vertical double-dashed lines indicate the GFED period. Years when the CESM2-LE and the CESM2-BB are statistically different at the 95% significance level are indicated with a thicker ensemble mean line and are determined using a two-sample Welch’s t-test. Note that the range of values on the y-axis varies across all panels.

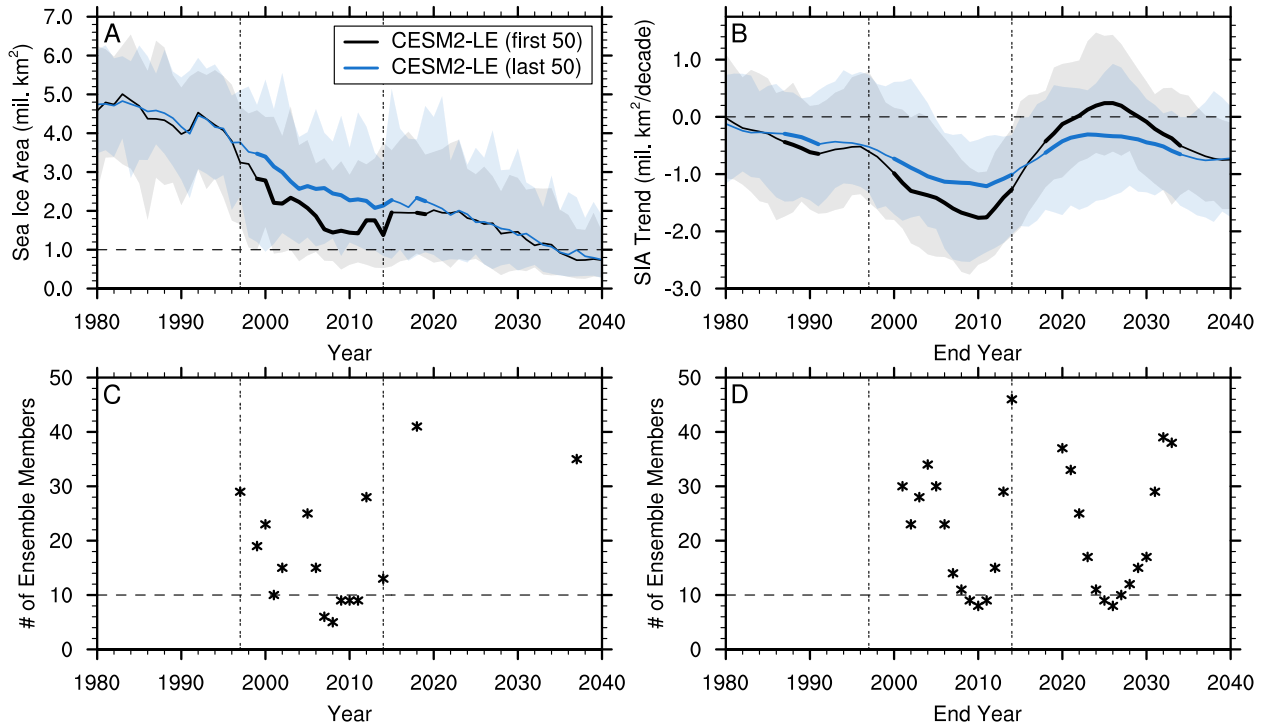


Fig. S2. Minimum number of ensemble members needed to detect a forced response to the homogenized BB emissions. September sea ice area (SIA) (A) anomalies relative to the 1940–1969 average and (B) 20-year linear trends in the first and last 50 members of the CESM2-LE. The ensemble mean is shown by the solid line and the full ensemble range is shown by the shading. Years when the first 50 and last 50 ensembles are statistically different at the 95% significance level are indicated with a thicker ensemble mean line and are determined using a two-sample Welch’s t-test. Minimum number of ensemble members needed for the September SIA (C) anomalies relative to the 1940–1969 average and (D) 20-year linear trends between the first 50 and last 50 ensembles to be statistically different at the 95% significance level. This is done by bootstrapping the two ensembles 10,000 times with a sub-sample size varying from 2 to 50. The horizontal dashed line indicates no anomalies in (A), no trend in (A), and 10 ensemble members in (C and D), and the two vertical double-dashed lines indicate the GFED period. In (B and D), values on the x-axis indicate the end year of the 20-year period over which the linear trend is computed.

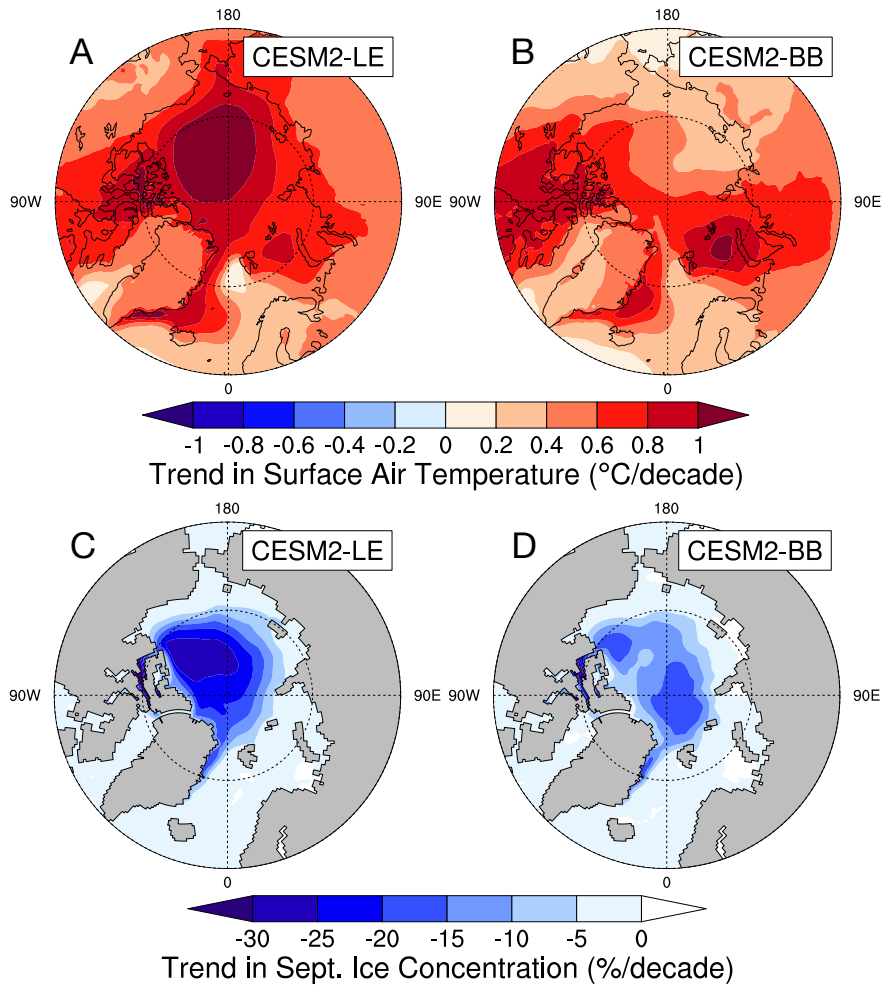


Fig. S3. Spatial patterns of BB impacts. Spatial distribution of the linear trend in (A and B) annual surface air temperature and (C and D) September sea ice concentration over the GFED period (1997–2014) in (A and C) the CESM2-LE and (B and D) the CESM2-BB.

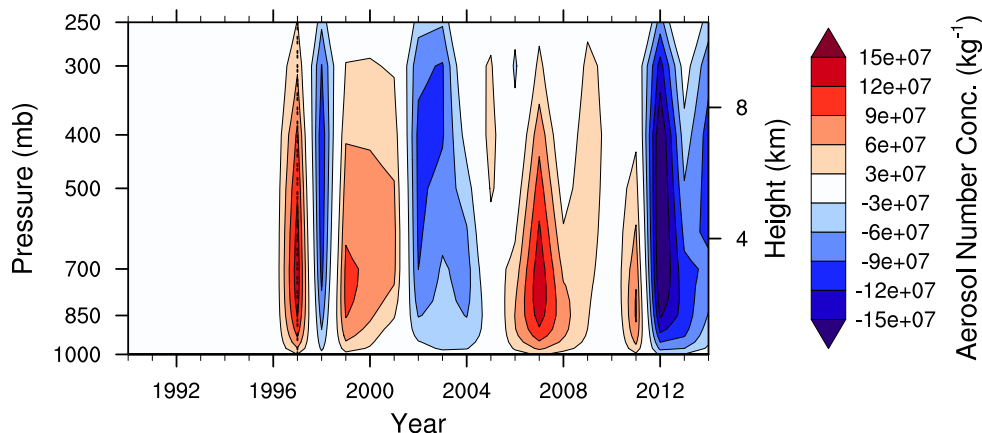


Fig. S4. BB emissions impact on Arctic primary carbon aerosols. Difference (CESM2-BB – CESM2-LE) in Arctic (70–90°N) summer (JJA) number concentration of aerosols in the primary carbon mode with height. Positive differences (red) indicate larger values in the CESM2-BB and negative differences (blue) indicate larger values in the CESM2-LE. The vertical double-dashed line indicates the start of the GFED period.

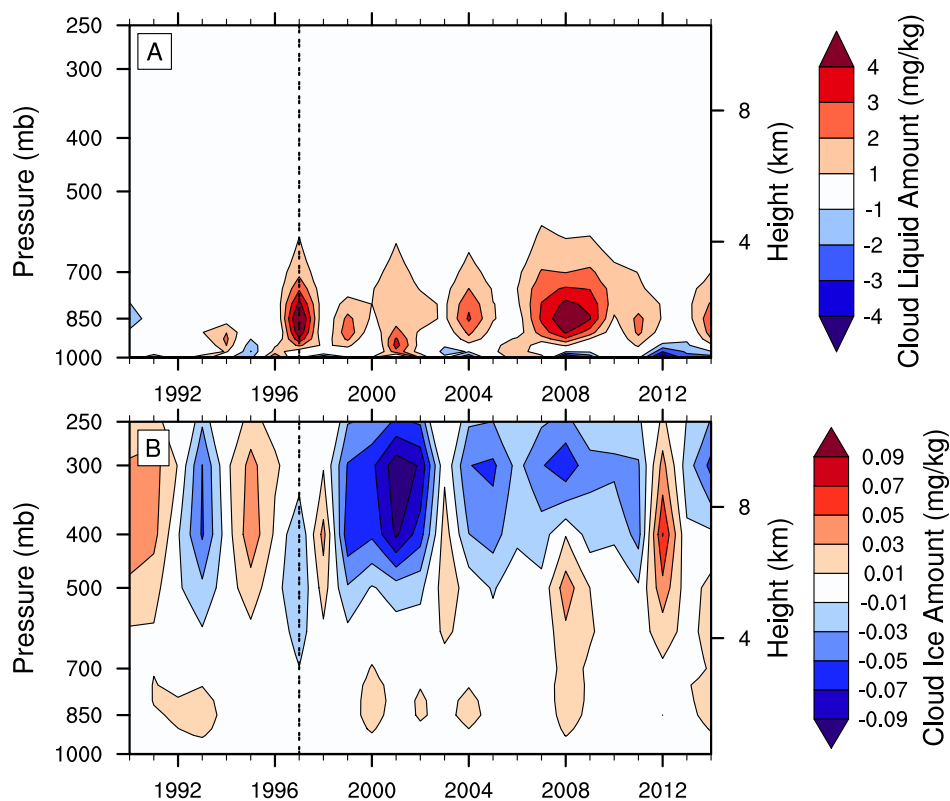


Fig. S5. BB emissions impact on Arctic liquid and ice clouds. Difference (CESM2-BB – CESM2-LE) in Arctic (70–90°N) summer (JJA) cloud (A) liquid and (B) ice amount with height. Positive differences (red) indicate larger values in the CESM2-BB and negative differences (blue) indicate larger values in the CESM2-LE. The vertical double-dashed line indicates the start of the GFED period. Note the same units but different range of the colorbar for each panel.

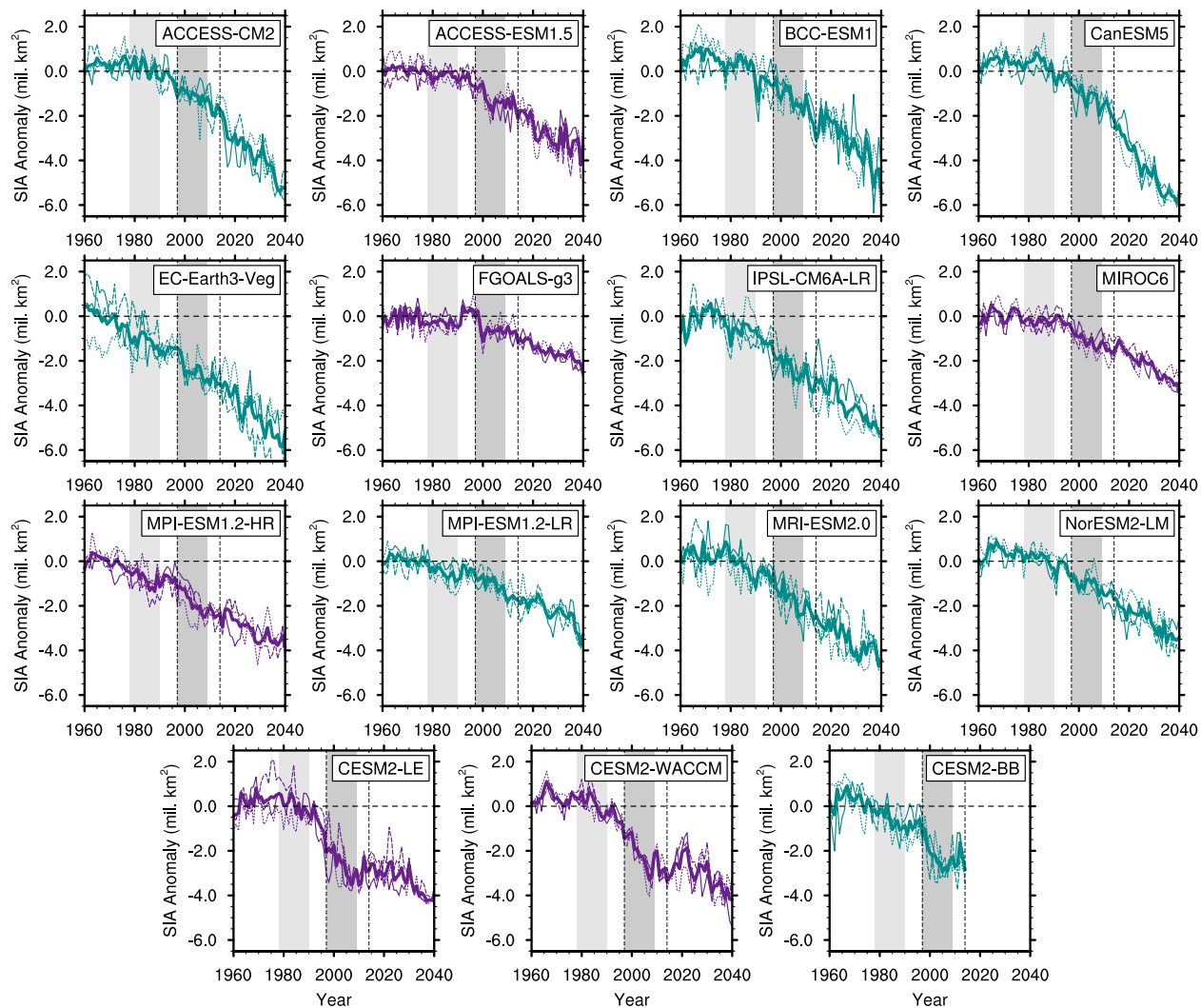


Fig. S6. September sea ice evolution in CMIP6 models. September sea ice area (SIA) anomalies relative to the 1940–1969 average for each CMIP6 model. Models in the sensitive category are shown in purple and the ones in the not sensitive category are shown in turquoise. For each model, the first three ensemble members are shown as thin lines and the ensemble mean is shown by the thick line. The light gray shaded region corresponds to the reference period 1978–1990 and the dark gray shaded region corresponds to the acceleration period 1997–2009 (see Materials and Methods for more details). The horizontal dashed line indicates no anomalies and the two vertical double-dashed lines indicate the GFED period. The last row shows the CESM2-LE, the CESM2-WACCM and the CESM2-BB for comparison, only using the first three ensemble members.

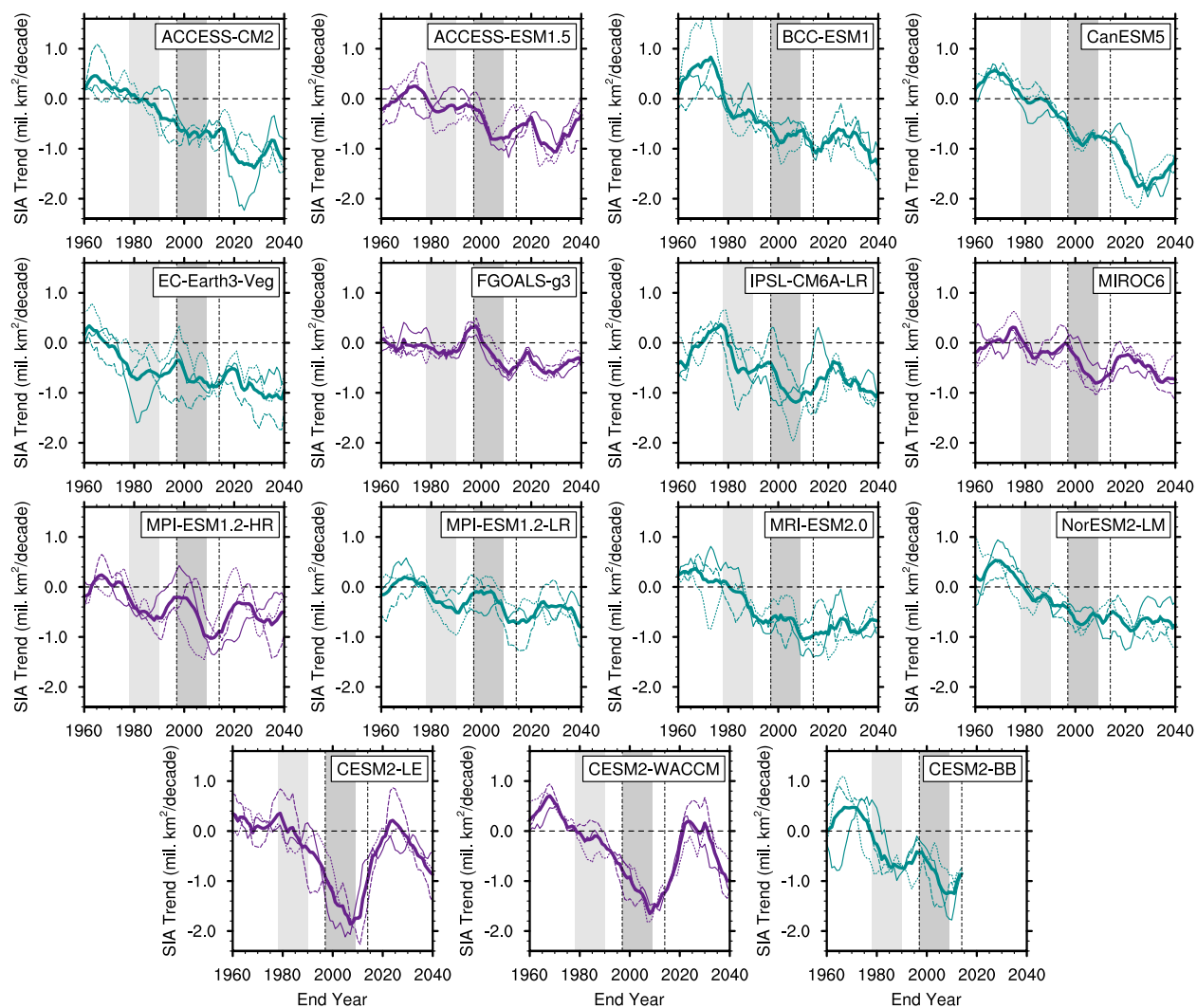


Fig. S7. September sea ice area trends in CMIP6 models. As in Fig. S6, but for 20-year linear trends in September sea ice area (SIA). The horizontal dashed line indicates no trend. Values on the x-axis indicate the end year of the 20-year period over which the linear trend is computed.